Published for SISSA by Springer

Received: *September 18, 2024*
Accepted: *October 26, 2024*
Published: *November 19, 2024*

Gravitational Bremsstrahlung in black-hole scattering at $\mathcal{O}(G^3)$: linear-in-spin effects

Lara Bohnenblust,[a] **Harald Ita**,[a,b] **Manfred Kraus**[c] **and Johannes Schlenk**[a]

[a] *Department of Astrophysics, University of Zurich, Winterthurerstrasse 190, 8057 Zurich, Switzerland*
[b] *Paul Scherrer Institut, CH-5232 Villigen PSI, Switzerland*
[c] *Departamento de Física Teórica, Instituto de Física, Universidad Nacional Autónoma de México, Cd. de México C.P. 04510, México*

E-mail: lara.bohnenblust@uzh.ch, harald.ita@psi.ch, mkraus@fisica.unam.mx, johannes.schlenk@psi.ch

Abstract: We compute the far-field time-domain waveform of the gravitational waves produced in the scattering of two spinning massive objects. The results include linear-in-spin (S) couplings and first-order gravitational corrections (G^3), and are valid for encounters in the weak-field regime. Employing a field-theory framework based on the scattering of massive scalar and vector particles coupled to Einstein-Hilbert gravity, we derive results for leading and the next-to-leading spectral waveforms. We provide analytic expressions for the required scattering data, which include trees, one-loop amplitudes and their cuts. The expressions are extracted from numerical amplitude evaluations with the Caravel program, using analytic reconstruction techniques applied in the classical limit. We confirm a recent prediction for infrared physics of the classical observable, and observe the surprising appearance of a ultraviolet singularity, which drops out in the far-field waveform.

Keywords: Scattering Amplitudes, Black Holes, Classical Theories of Gravity

ArXiv ePrint: 2312.14859

https://doi.org/10.1007/JHEP11(2024)109

Contents

1 Introduction **1**

2 Notation and conventions **4**
- 2.1 Classical scaling limit 5
- 2.2 Spin operators 7
- 2.3 Vector-boson states 9
- 2.4 Graviton states 10

3 Waveform observable from amplitudes **11**

4 Scattering amplitudes computation **14**
- 4.1 Organization of the computation 15
- 4.2 Brief review of numerical unitarity 16
- 4.3 Form-factor decomposition 17
- 4.4 Classical limit of quantum amplitudes 19
- 4.5 Analytic reconstruction 21

5 Results **22**
- 5.1 Leading-order amplitudes 22
- 5.2 Next-to-leading order waveform 23
- 5.3 Analytic properties 27

6 Fourier transformation **28**

7 Validation **30**

8 Conclusion **31**

A Field theory **32**

B Feynman integrals **34**

C IR divergence of waveform observable **38**

D Momentum parameterization **39**

1 Introduction

In recent years, the groundbreaking detection of gravitational waves [1, 2] has opened a new frontier in astrophysics, providing new and revolutionary means to explore the universe and unlock profound insights into the nature of spacetime itself. Future upgrades of the existing gravitational-wave observatories of the LIGO-Virgo-KAGRA collaboration [3] and planned

JHEP11(2024)109

observatories such as Cosmic Explorer [4], Einstein Telescope [5] and LISA [6], operating in lower frequency ranges will explore new types of systems including fly-bys, captures, eccentric configurations and high spin. To fully exploit the physics potential of the observatories, it will be important to increase the theoretical precision and scope of gravitational waveform predictions in the near future.

The central challenge in obtaining a waveform of binary systems is the non-linearity of the gravitational interaction coupled with the dependence on multiple physical scales. Present theoretical predictions rely on numerical relativity [3] and the effective-one-body (EOB) formalism [7, 8], based on input from post-Newtonian (PN) dynamics [9, 10], the gravitational self-force formalism [11, 12], the non-relativistic general-relativity (NRGR) [13–17] or the weak-field Post-Minkowskian (PM) approximation [18–27].

In contrast, we focus here on a first-principle waveform computation in the PM expansion, which we derive to next-to-leading order in the Newton constant G, i.e. to order $\mathcal{O}(G^3)$. This perturbative approach allows us to systematically compute dynamics and observables of binary black-hole systems and is applicable in a weak-field regime and at large eccentricities. The PM approach has rapidly advanced in recent years starting from its initial application in General Relativity [19–26, 28]. In particular the recent use of modern field-theory methods has led to impressive high-order $\mathcal{O}(G^3)$ [29] and $\mathcal{O}(G^4)$ [30–34] predictions for classical quantities, and has already helped to improve resummation of the effective-one-body (EOB) Hamiltonians [35, 36]. It has further fueled the developement of the heavy-mass effective field theory (HEFT) [37–40], worldline EFTs [32–34, 41–43] and eikonal approaches [44–47]. As far as the waveform is concerned, methods are available to directly link this observable to scattering amplitudes (KMOC) [48–50] and to worldline quantum field theory (WQFT) [51–53]. By now, early classical results [54, 55] have been reproduced for the scattering of two Schwarzschild black holes at leading-order $\mathcal{O}(G^2)$, and were recently extended to the next-to-leading order $\mathcal{O}(G^3)$ [56–59]. The importance of the so-called cut contribution to this observable for imposing classical causality was pointed out in [60]. This contribution will likely be crucial for a comparison with the multipolar PM waveform [61]. Recently such a comparison, including cut contributions, was reported for the limit of soft radiation [62].

A further motivation for this work is to consider spin effects in the waveform observable, as required for describing astrophysical black holes. The foundational work on the PM treatment of spin [63–66] has sparked many conceptional and computational developments, and has exposed new links between field theory and GR [67, 68]. Focusing on perturbative computations, spin corrections to two-body dynamic have by now been obtained up to $\mathcal{O}(G^4)$ in worldline approaches [42, 69, 70] and at $\mathcal{O}(G^3)$ in field theory [71]. The latter obtains spin corrections from massive field theories [72–80] via effective field theory [66] or via scattering amplitudes using a generalization of the KMOC formalism [49, 81]. However, how to construct the right field theory, that mirrors the properties of Kerr black holes, remains an open question. At low spin orders minimally coupled theories correctly capture the spin couplings of macroscopic objects [82]. This 'spin universality' property, was validated for the minimally coupled vector theory up to quadratic-in-spin multipoles at $\mathcal{O}(G^3)$ [71]. Turning to the waveform observable, $\mathcal{O}(G^2)$ quadratic spin effects were obtained in ref. [52] and to higher-spin order [83–85], recently. Beyond the leading PM order, the spin-dependent memory effect is known at $\mathcal{O}(G^3)$ [85].

JHEP11(2024)109

The goal of this article is to present the spectral waveform emitted by two colliding black holes including $\mathcal{O}(G^3)$ corrections, and to include linear-in-spin effects. We provide analytic results in terms of momentum-transfer variables and in frequency space. Furthermore, we present exemplary plots of the gravitational waveform in the time and position-space domain, and demonstrate the impact of the cut contribution in the gravitational waveform. The waveform observable is computed from first principles in QFT following the KMOC formalism [48, 50]. We exploit the classical limiting procedure and the detailed analytic and physical understanding of refs. [56–59], but let QFT do its work. We provide an independent computation of the necessary Feynman integrals and one-loop scattering data. In addition, we provide the cut contribution, that allows us to obtain the full non-spinning waveform at $\mathcal{O}(G^3)$.

Building on these results, we extend this study by including linear-in-spin effects, which we extract from a one-loop computation including massive vectors and scalars. This approach exploits the relation between minimally coupled vector-field theory and spinning point-particles [82, 86–88]. Recently, a similar approach has been pursued in the analysis of the $\mathcal{O}(G^3)$ conservative dynamics quadratic in spin [71], which we build on.

We present a purely numerical approach to obtain analytic results to handle the multi-scale computation. The KMOC formalism relates the waveform observable at $\mathcal{O}(G^3)$ to tree-level and one-loop scattering amplitudes and their cuts. We obtain all scattering data with the Caravel-program [89], which implements exact numerical evaluations using modular arithmetic. The program allows to efficiently handle the intricate gravitational coupling structure of the massive scalar and vector fields. At tree-level, the program yields numerical scattering amplitudes through Berends-Giele recursions [90], using interaction vertices obtained with xAct [91, 92]. At loop-level, the program implements the numerical unitarity method [93–97] in the variant of refs. [98–100], which provides numerical values for the rational integral coefficients of a one-loop integral basis. We employ functional reconstruction techniques [101, 102] to obtain analytic expressions in the classical expansion parameter and isolate the classical terms. The full analytic expressions are obtained using the functional-reconstruction method [99, 101] in finite-field arithmetic [102]. An important aspect of computing spin corrections is the relation between polarization states of vector fields and classical spin variables. We obtain this map, by introducing a form-factor decomposition [71], which we then link to classical spin multi poles [77]. We anticipate that this setup will allow to obtain further higher-spin corrections to the $\mathcal{O}(G^3)$ waveform, which we leave for future work.

We make a number of interesting observations. For instance, we confirm the recent predictions for the IR-singularities of the waveform observable [60] and link their result to a modification of the Weinberg's IR-theorem [103]. Furthermore, we observe an additional contribution to the $1/\epsilon$-pole in the dimensional regulator in the cut contribution, which we attribute to the UV. The UV pole is shown to integrate to zero in the Fourier transformation to position-space in the far-field asymptotic waveform. In the light of the recent comparisons with previous results for the gravitational waveform in the Post-Newtonian expansion [61, 62], we provide a new input for the scalar and for the linear-in-spin waveform at $\mathcal{O}(G^3)$.

The article is organized as follows. In section 2, we establish our notation and present our conventions for spin operators and polarization states of gravitons and massive vector fields. Next, in section 3, we give a brief overview how the gravitational waveform can be related

JHEP11(2024)109

to scattering amplitudes. In section 4, we explain in detail how the necessary scattering amplitudes are computed. We put special emphasis on the description of our exact numerical approach to obtain amplitudes in the classical limit. In section 5, we collect our analytical results and discuss various analytical features we observe. Furthermore, in section 6, we elaborate the computation of the position-space waveform and show some numerical results for the gravitational waveform. Finally, in section 8, we give our conclusions and an outlook.

2 Notation and conventions

We study gravitational radiation in classical two-body scattering far from the source. Some of the classical bodies are assumed to carry spin. We employ a QFT approach to describe the classical system by coupling matter fields to Einstein-Hilbert gravity,

$$\mathcal{L} = \mathcal{L}_{\text{EH}} + \mathcal{L}_{\text{matter}}. \tag{2.1}$$

The classical information is then extracted from quantum scattering amplitudes by considering them in a scaling limit, referred to as the *classical limit*. For the Einstein-Hilbert Lagrangian we follow the conventions,

$$\mathcal{L}_{\text{EH}} = -\frac{2}{\kappa^2}\sqrt{|g|}R, \tag{2.2}$$

where $g = \det(g_{\mu\nu})$ and R the is Ricci-scalar defined by $R = R^{\rho}{}_{\mu\rho\nu}\, g^{\mu\nu}$. Further details on the definition of the Riemann-tensor are given in appendix A. We work in the 't Hooft-Veltman (HV) scheme of dimensional regularization using $D = 4 - 2\epsilon$ and setting the dimension of the tensor algebra D_s to the same value, i.e. $D_s = 4 - 2\epsilon$. Furthermore, we work with weak gravitational fluctuations around a flat background $\eta_{\mu\nu}$. The fluctuations are described by the graviton field $h_{\mu\nu}$ in the decomposition,

$$g_{\mu\nu} = \eta_{\mu\nu} + \kappa\, h_{\mu\nu}\,. \tag{2.3}$$

We work in the mostly-minus metric convention $\eta = \text{diag}\{1, -1, -1, -1\}$ and use the gravitational coupling $\kappa = \sqrt{32\pi G}$ in terms of the Newton constant $G = \hbar G_N/c^3$, where c is the speed of light, $\hbar$ the Planck constant and $x^0 = ct$.

Massive point-like sources are described by minimally-coupled field theories of a massive scalar ϕ or a vector-field V_μ with Lagrangians,

$$\mathcal{L}_{(\phi,m)} = \frac{1}{2}\sqrt{|g|}\Big[g^{\mu\nu}(\partial_\mu\phi)(\partial_\nu\phi) - m^2\phi^2\Big], \tag{2.4}$$

$$\mathcal{L}_{(V,m)} = -\frac{1}{4}\sqrt{|g|}\Big[g^{\mu\rho}g^{\nu\sigma}F_{\mu\nu}F_{\rho\sigma} - 2m^2 g^{\mu\nu}V_\mu V_\nu\Big]\,, \quad F_{\mu\nu} = \partial_\mu V_\nu - \partial_\nu V_\mu. \tag{2.5}$$

The massive objects are represented as fundamental states of field theories, and we associate the objects' intrinsic angular momentum to the fields' spin representations. The mass parameter m in the Lagrangian corresponds to the physical mass.

In the following, we study two types of systems: scalar and spinning compact objects. The scattering of spin-less point-particles is described by the matter Lagrangian,

$$\mathcal{L}^{(i)}_{\text{matter}} = \mathcal{L}_{(\phi_1,m_1)} + \mathcal{L}_{(\phi_2,m_2)}. \tag{2.6}$$

JHEP11(2024)109

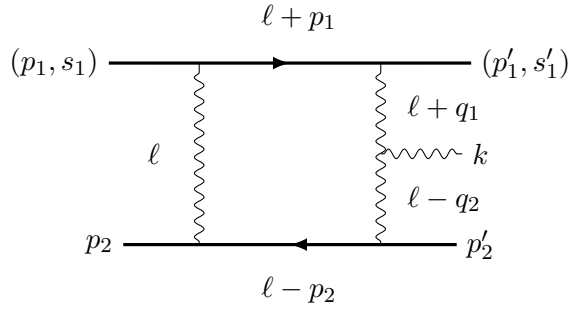

Figure 1. Scattering process of two massive compact objects (solid lines), emitting gravitational radiation (wavy line). Spin is indicated, as well as a diagrammatic representation of the exchange of gravitons to order κ^5 in perturbation theory.

To describe spinning point particles, we take advantage of the observation [82] that the scattering amplitudes involving minimally coupled spin-s massive particles can be used to extract classical-spin multipoles up to S^{2s}, i.e. $2s$ powers of the classical spin S. Therefore, we consider a massive vector field and a massive scalar, given by

$$\mathcal{L}^{(ii)}_{\text{matter}} = \mathcal{L}_{(V,m_1)} + \mathcal{L}_{(\phi_2,m_2)}. \tag{2.7}$$

Our conventions for creation and annihilation operators as well as polarization states are collected in appendix A.

In the above theories, we study the scattering process of four massive scalar particles and one graviton,

$$\text{i}: \quad \phi_1(p_1) + \phi_2(p_2) \to \phi_1(p_1') + \phi_2(p_2') + h(k^s)\,, \tag{2.8}$$

and the scattering of two massive vector particles and two scalar particles,

$$\text{ii}: \quad V(p_1^{s_1}) + \phi_2(p_2) \to V(p_1'^{\,s_1'}) + \phi_2(p_2') + h(k^s)\,, \tag{2.9}$$

respectively. Here the superscripts s_1 and s_1' denote the spin quantum numbers of the vector particles. The helicity of the graviton field h is labeled by the superscript s. The momenta p_1 and p_2 are understood as incoming, and the final-state momenta p_1', p_2' and k are given in the out-going convention. These kinematic conventions are summarized in figure 1.

2.1 Classical scaling limit

We are concerned with the perturbative expansion in G of the classical scattering of two macroscopic rotating objects (large spin and mass) and the emission of a classical, long wavelength gravitational wave. The objects are assumed structureless, such as black holes. We start our computation in a second-quantized field theory and will take limits to retrieve such point-particle interaction in the weak-field expansion.

The kinematic properties of the corresponding scattering process are exposed in the barred or soft variables [104–106],

$$\begin{aligned} p_1 &= \bar{m}_1 u_1 + \frac{q_1}{2}, \qquad p_1' = \bar{m}_1 u_1 - \frac{q_1}{2}, \\ p_2 &= \bar{m}_2 u_2 + \frac{q_2}{2}, \qquad p_2' = \bar{m}_2 u_2 - \frac{q_2}{2}, \qquad k = q_1 + q_2, \end{aligned} \tag{2.10}$$

JHEP11(2024)109

where $p_1^2 = p_1'^2 = m_1^2$, $p_2^2 = p_2'^2 = m_2^2$ and $k^2 = 0$. Here u_i denote normalized ($u_i^2 = 1$) four velocities and the on-shell conditions of initial and final states imply $q_i \cdot u_i = 0$. Similarly $k^2 = (q_1+q_2)^2 = 0$ yields $q_1 \cdot q_2 = -(q_1^2+q_2^2)/2$. The auxiliary mass parameters $\bar{m}_i$ are related to the physical masses through $\bar{m}_i^2 = m_i^2 - q_i^2/4$. We will also use the impact parameter four vectors b_i which are Fourier conjugate to the momenta q_i. The interpretation of the momenta is as follows: the four-velocities u_i represent classical velocities of the scattering objects, and q_i (small) momentum transfer during their interaction. Part of the exchanged momentum $k = q_1 + q_2$ is emitted as radiation.

We use seven Lorentz invariant inner products to parameterize the kinematic space,

$$\begin{aligned} &y = u_1 \cdot u_2, \qquad \omega_1 = -u_1 \cdot k, \qquad \omega_2 = -u_2 \cdot k, \\ &q_1^2, \quad q_2^2, \qquad \bar{m}_1^2 \quad \text{and} \quad \bar{m}_2^2. \end{aligned} \tag{2.11}$$

In the physical region of the phase space the invariants fulfill the constraints

$$y > 1, \qquad q_i^2 < 0, \qquad \omega_i < 0, \qquad \bar{m}_i > 0. \tag{2.12}$$

In the scattering process, the weak-field classical dynamic appears in the following regime in field theory [29, 107]. The weak-field expansion is a perturbative expansion in

$$\frac{\kappa^2 m_i}{|\vec{b}_j|} \ll 1\,. \tag{2.13}$$

To ensure gravitational interaction of the masses we impose their effective gravitational couplings to be large,

$$\kappa\, m_i \gg 1\,. \tag{2.14}$$

This is equivalent to the non-perturbative condition that the Schwarzschild radius of the masses is much larger than their Compton wave lengths, $\kappa^2\, m_i \gg 1/m_i$. In terms of momentum variables the above constraints imply that the gravitational interaction is long wavelength,

$$\frac{k^\mu}{m_i} \sim \frac{q_j^\mu}{m_i} \ll 1\,, \tag{2.15}$$

and weak,

$$\kappa\, q_i^\mu \sim \kappa\, k^\mu \ll 1\,, \tag{2.16}$$

compared to the matter-gravity interaction. Accordingly, in field-theory diagrams interactions with comparable momentum $\ell \sim q_i, k$ are suppressed relative to the ones including matter lines.

Finally, the objects spin (S_i) is assumed to be macroscopic and comparable in size to the angular momentum $\vec{L}$ of the system,

$$|\vec{S}_i| \sim |\vec{L}_i| = |\vec{p}_i \times \vec{b}_i|\,. \tag{2.17}$$

At the same time a perturbative expansion in spin requires the ring-radius $a_i^\mu = S_i^\mu/m_i$ to be much smaller than the objects' Schwarzschild radius,

$$|\vec{a}_i| = |\vec{S}_i/m_i| \ll \kappa^2\, m_i\,. \tag{2.18}$$

JHEP11(2024)109

To implement the classical point-particle limit, we introduce the mass ratio q,

$$q = \frac{\bar{m}_2}{\bar{m}_1}, \quad \bar{m}_1 = \bar{m}, \quad \bar{m}_2 = \bar{m}\, q. \tag{2.19}$$

The classical limit is then a scaling limit in the variable $\bar{m} \to \infty$ and amounts to performing a series expansion around infinite mass $\bar{m}$,

$$\bar{m} \to \infty \quad \text{with} \quad y\,, q_i^2\,, q\,, \omega_i\,, \frac{S_i}{\bar{m}}\,, \sqrt{\bar{m}}\kappa = \text{fixed}. \tag{2.20}$$

An equivalent scaling limit via $\hbar$ counting [49], is obtained by rescaling all dimensionful quantities (including κ) simultaneous to the limit (2.20), such that the mass-parameters m_i remain fixed. For completeness we give this scaling transformation,

$$\hbar \to 0 \quad \text{with} \quad \bar{m}, y\,, \frac{q_i^2}{\hbar^2}\,, q\,, \frac{\omega_i}{\hbar}\,, \hbar S_i\,, \sqrt{\hbar}\kappa = \text{fixed}. \tag{2.21}$$

In our presentation we will rely on the former formulation (2.20) of the limiting procedure.

In the classical limit, L-loop five-point scattering amplitudes including four massive particles and one graviton have a well defined scaling in $\bar{m}$ and κ. For the order n_s spin multipole contribution we have

$$M^{n_s} \sim \kappa^{3+2L}\, \bar{m}^{4+L}\, (S/\bar{m})^{n_s}\,. \tag{2.22}$$

The dependence on κ follows from Feynman rules. The dependence on $\bar{m}$ and S produces the same leading scaling as the $M^{n_s=0}$ amplitude in the large-$\bar{m}$ and $S/\bar{m}$ = fixed limit. The scalar amplitude scales like a fan-diagram [29, 108, 109], including $\bar{m}^2$ for each matter-graviton vertex, and $1/\bar{m}$ for massive propagators. We expect the scaling behavior,

$$M^{\text{tree},n_s} \sim \kappa^3\, \bar{m}^4\, (S/\bar{m})^{n_s}\,, \qquad M^{1-\text{loop},n_s} \sim \kappa^5\, \bar{m}^5\, (S/\bar{m})^{n_s}\,. \tag{2.23}$$

We refer to terms with the expected scaling dependence $\bar{m}^{n_c}$ as classical scaling. Slower growth $\bar{m}^{n<n_c}$ will be called quantum and faster growth $\bar{m}^{n>n_c}$ hyper-classical. Hyper-classical scaling often appears in intermediate computational steps and drops out in properly defined observables.

2.2 Spin operators

We compute scattering amplitudes which serve as building blocks of asymptotic field-theory observables. The classical spin dependence of the observables is determined by making their dependence on spin operators manifest. In the following, we briefly review the properties of spin operators.

The relativistic spin operator for a state with momentum p and mass m ($p^2 = m^2$) is the Pauli-Lubanski operator (see e.g. [110]), which is given as

$$\mathbb{S}_\mu = \frac{1}{2m} \epsilon_{\mu\nu\alpha\beta}\, p^\nu \mathbb{M}^{\alpha\beta}\,, \tag{2.24}$$

for the Lorentz-group generators $\mathbb{M}^{\rho\sigma}$,

$$\left[\mathbb{M}^{\mu\nu}, \mathbb{M}^{\rho\sigma}\right] = i(\eta^{\nu\rho}\, \mathbb{M}^{\mu\sigma} - \eta^{\mu\rho}\, \mathbb{M}^{\nu\sigma} - \eta^{\nu\sigma}\, \mathbb{M}^{\mu\rho} + \eta^{\mu\rho}\, \mathbb{M}^{\mu\sigma})\,, \tag{2.25}$$

and where $\epsilon_{\mu\nu\alpha\beta}$ is the Levi-Civita tensor with $\epsilon^{0123} = 1$.

JHEP11(2024)109

As we are working with spin-1 vector fields we only need the Lorentz-group generators in the corresponding vector representation. We will specialize to this case from now on and the generators explicitly read

$$(\mathbb{M}^{\mu\nu})^{\alpha}{}_{\beta} = i(\eta^{\mu\alpha}\delta^{\nu}{}_{\beta} - \eta^{\nu\alpha}\delta^{\mu}{}_{\beta})\,. \tag{2.26}$$

The Pauli-Lubanski operators are transverse,

$$\mathbb{S}_{\mu}\, p^{\mu} = 0, \tag{2.27}$$

due to the anti-symmetry of $\epsilon_{\mu\nu\rho\sigma}$. Furthermore, they are also transverse, viewed as tensors in their representation indices,

$$(\mathbb{S}_{\mu})^{\alpha}{}_{\beta}\, p^{\beta} = p_{\alpha}(\mathbb{S}_{\mu})^{\alpha}{}_{\beta} = 0\,. \tag{2.28}$$

This property follows from the vector representation of the Lorentz generators (2.26) and their contraction with $p^{\nu}\epsilon_{\mu\nu\rho\sigma}$.

For completeness we collect the commutator algebra of the Pauli-Lubanski operators

$$\left[\mathbb{S}^{\mu}, \mathbb{S}^{\nu}\right] = -i\epsilon^{\mu\nu\rho\sigma}\mathbb{S}_{\rho}\frac{p^{\sigma}}{m}\,. \tag{2.29}$$

In particular, for a state at rest $p = (m, 0, 0, 0)$, the $\mathbb{S}^{i}$ form the $so(3)$ Lie algebra of the respective little group. For this momentum choice, $\mathbb{S}_{0}$ vanishes and the momentum p is in the kernel of $\mathbb{S}^{i}$. The polarization states for a fixed momentum form irreducible representations of the Pauli-Lubanski operators.

Finally, we will require the projection operator

$$\mathbb{P}^{\alpha}_{\beta} = \delta^{\alpha}{}_{\beta} - \frac{p^{\alpha}p_{\beta}}{m^{2}}\,, \tag{2.30}$$

which projects into the subspace transverse to the timelike momentum p. The Pauli-Lubanski operators $\mathbb{S}^{\mu}$, the projector $\mathbb{P}^{\alpha}{}_{\beta}$, as well as the massive polarization states $\varepsilon_{v\mu}(p)$ (with $\varepsilon_{v}(p)\cdot p = 0$) all are non-vanishing in the subspace transverse to p.

To make manifest the observables' dependence on spin, we will use a form-factor decomposition which expresses amplitudes in terms of a complete basis of spin operators and the transverse projector. In fact, the vector representation operators

$$\mathbb{P}^{\alpha}{}_{\beta}\,, \quad (\mathbb{S}^{\mu})^{\alpha}{}_{\beta} \quad \text{and} \quad (\mathbb{S}^{\{\mu}\mathbb{S}^{\nu\}})^{\alpha}{}_{\beta}, \tag{2.31}$$

form an over-complete basis of rank two, transverse tensors, which can be verified in the rest frame $p = (m, 0, 0, 0)$. Here we take the indices μ and ν as labels and the representation indices (α, β) as the mentioned tensor indices. Furthermore, we defined the symmetric-traceless tensor

$$\mathbb{S}^{\{\lambda}\mathbb{S}^{\kappa\}} \equiv \frac{1}{2}\left(\mathbb{S}^{\lambda}\mathbb{S}^{\kappa} + \mathbb{S}^{\kappa}\mathbb{S}^{\lambda}\right) - \frac{1}{3}(\mathbb{S}\cdot\mathbb{S})\,\mathbb{P}^{\lambda\kappa}. \tag{2.32}$$

JHEP11(2024)109

2.3 Vector-boson states

An important fact is that the spin operators are non-vanishing in the transverse space. Consequently, we set up the form-factor decomposition with respect to polarization states which take values in the same transverse space, that is polarization states associated to the same momentum.

To make this structure manifest, we define polarization states of all massive vector states with respect to the common momentum p with $p^2 = m^2$. For a state with momentum $(p-q)$ with $(p-q)^2 = m^2$ we have

$$\varepsilon_{v\mu}(p-q) = \Lambda_\mu{}^\nu(p-q,p)\,\varepsilon_{v\nu}(p)\,, \tag{2.33}$$

using the Lorentz-boost $\Lambda^\mu{}_\nu$,

$$\Lambda^\mu{}_\nu(p-q,p) = \delta^\mu{}_\nu + \frac{1}{q^2-4m^2}\left[2\frac{q^2}{m^2}(p-q)^\mu\,p_\nu + 4q^\mu\,p_\nu - 4\left(p-\frac{q}{2}\right)^\mu q_\nu\right], \tag{2.34}$$

which gives $(p-q)^\mu = \Lambda^\mu{}_\nu\,p^\nu$. Note that the little-group indices v of the polarization vector $\varepsilon_{v\mu}(p)$ are unchanged. Outer products of vector-boson states associated to the same momentum are transverse tensors and can be expressed in terms of a basis of spin operators (2.31), likewise the physical transverse part of the amplitude. A tensor decomposition of a spin amplitude $M^{v'v}$ is then

$$\begin{aligned} M^{v'v} &= M^\mu_{\ \rho}\,\Lambda_\mu{}^\nu(p-q,p)\,\bar\varepsilon_{v'\nu}(p)\,\varepsilon_v^\rho(p) \\ &\to \quad M^\mu_{\ \rho}\,\Lambda_\mu{}^\nu(p-q,p) = c\,\mathbb{P}^\nu{}_\rho + c_\lambda(\mathbb{S}^\lambda)^\nu{}_\rho + c_{\lambda\kappa}(\mathbb{S}^{\{\lambda}\mathbb{S}^{\kappa\}})^\nu{}_\rho, \end{aligned} \tag{2.35}$$

In order to obtain this decomposition, we will first introduce an auxiliary tensor basis, which we relate to classical spin vectors in a second step.

The basis is constructed with three transverse vectors

$$v_i \in \{\mathbb{P}\cdot q_1, \mathbb{P}\cdot q_2\,, \mathbb{P}\cdot u_2\}\,, \tag{2.36}$$

where we project three vectors which are linear independent of p. We use the following rank-two tensor basis,

$$\begin{aligned} \{T_1^{\alpha\beta},\ldots,T_9^{\alpha\beta}\} = \Big\{&\mathbb{P}^{\alpha\beta}, v_1^{[\alpha}v_2^{\beta]}, v_1^{[\alpha}v_3^{\beta]}, v_2^{[\alpha}v_3^{\beta]}, \\ &v_1^{\{\alpha}v_2^{\beta\}}, v_2^{\{\alpha}v_3^{\beta\}}, v_1^{\{\alpha}v_3^{\beta\}}, v_1^{\{\alpha}v_1^{\beta\}}, v_2^{\{\alpha}v_2^{\beta\}}\Big\}. \end{aligned} \tag{2.37}$$

where we use the convention

$$v_i^{[\alpha}v_j^{\beta]} = \frac{1}{2}\left[v_i^\alpha v_j^\beta - v_i^\beta v_j^\alpha\right], \tag{2.38}$$

$$v_i^{\{\alpha}v_j^{\beta\}} = \frac{1}{2}\left[v_i^\alpha v_j^\beta + v_i^\beta v_j^\alpha\right] - \frac{1}{3}(v_i\cdot v_j)\,\mathbb{P}^{\alpha\beta}. \tag{2.39}$$

When contracted with explicit polarization states we obtain

$$T_n^{v'v} = \bar\varepsilon_{v'}(p-q)\cdot T_n\cdot\varepsilon_v(p) = \bar\varepsilon_{v'}(p)\cdot[\Lambda(p,p-q)\cdot T_n]\cdot\varepsilon_v(p)\,. \tag{2.40}$$

Next we relate the tensor basis to functions in classical spin. One method is to use a Clebsch-Gordan decomposition of a product of polarization states [76],

$$\bar{\varepsilon}^{\mu}_{v'}(p)\varepsilon^{\nu}_{v}(p) = \frac{1}{3}\bar{\varepsilon}_{v'}\cdot\mathbb{P}\cdot\varepsilon_{v}\left(\eta^{\mu\nu}-\frac{p^{\mu}p^{\nu}}{m^2}\right)-\frac{i}{2m}\epsilon^{\mu\nu\rho\sigma}p_{\rho}\bar{\varepsilon}_{v'}\cdot\mathbb{S}_{\sigma}\cdot\varepsilon_{v}+\bar{\varepsilon}_{v'}\cdot\mathbb{S}^{\{\mu}\mathbb{S}^{\nu\}}\cdot\varepsilon_{v}\,, \quad (2.41)$$

which expresses the spin states in terms of a irreducible scalar, anti-symmetric and symmetric-traceless representation of the little group transformations. Motivated by the relation

$$\frac{\bar{\varepsilon}_{v}\cdot\mathbb{S}^{\mu}\cdot\varepsilon_{v}}{\bar{\varepsilon}_{v}\cdot\varepsilon_{v}}\to S^{\mu} \quad (2.42)$$

we obtain a simple replacement rule $T_n \to T_n^{\rm cl}$ which relates quantum-spin observables to classical ones,

$$T_n^{\rm cl}(S) = -\left[\Lambda(p,p-q)\cdot T_n\right]_{\mu\nu}\left[\frac{1}{3}\left(\eta^{\mu\nu}-\frac{p^{\mu}p^{\nu}}{m^2}\right)-\frac{i}{2m}\epsilon^{\mu\nu\rho\sigma}p_{\rho}S_{\sigma}+S^{\{\mu}S^{\nu\}}\right], \quad (2.43)$$

for the classical-spin vector S^{μ} with $S\cdot p=0$. Importantly we introduce an overall minus sign in eq. (2.43), since we remove inner product $\bar{\epsilon}_v\cdot\epsilon_v=-1$.[1]

2.4 Graviton states

In order to make the classical limit manifest, we use a form-factor decomposition for the graviton states. The graviton polarisation tensors are $\varepsilon_{\mu\nu}$, which we write as product states of two spin-1 fields. Using a basis of plus and minus polarized vectors, the polarization tensors of a circularly polarized gravitational wave are given by

$$\varepsilon^{\mu\nu}_{\pm2}(k) = \varepsilon^{\mu}_{\pm1}(k)\varepsilon^{\nu}_{\pm1}(k). \quad (2.44)$$

and hence fulfill the transversality condition $\varepsilon^{\mu\nu}_{\pm2}(k)\,k_{\mu}=\varepsilon^{\mu\nu}_{\pm2}(k)\,k_{\nu}=0$. The states are normalised as

$$\bar{\varepsilon}_{s\mu\nu}\varepsilon^{\mu\nu}_{s'}=\delta_{s's}\,,\quad \varepsilon^{\mu\nu}_{s}=\bar{\varepsilon}^{\mu\nu}_{-s}\,,\quad s,s'\in\{-2,2\}\,, \quad (2.45)$$

and are traceless, e.g. $(\varepsilon_s)_{\mu}{}^{\mu}=(\bar{\varepsilon}_s)_{\mu}{}^{\mu}=0$. In analytic computations, contractions of the graviton states with the linearly independent set of four vectors $\{u_1,u_2,k,q_1\}$ appear. As we are using product states, these factorize into two scalar products of a spin-1 polarization vector $\varepsilon^{\mu}_{\pm1}(k)$ with one of the independent momenta. Starting from 10 symmetric contractions, we can reduce to a minimal basis of only two quadratic monomials. First, we use the traceless condition which can be implemented by setting $(\varepsilon_s)^2=0$ together with the Gram determinant identity $\mathrm{G}(u_1,u_2,k,q_1,\varepsilon_h)=0$ to arrive at 9 independent monomials. Taking into account also transversality $\varepsilon_h\cdot k=0$, this set is reduced by 4 monomials. Next, we use the gauge freedom $\varepsilon_h\to\varepsilon_h+k$ to set inner products $\varepsilon_h\cdot u_1$ to zero,

$$u_1\cdot\varepsilon_h=0 \quad (2.46)$$

[1] This sign implies that the scalar component of the scalar-vector waveform matches the scalar-scattering waveform.

JHEP11(2024)109

We arrive at the fact that amplitudes including a single graviton emission can be given as linear combinations of the two monomials

$$F_1^{2h} = (\varepsilon_h \cdot u_2)\,(\varepsilon_h \cdot u_2)\,, \qquad F_2^{2h} = (\varepsilon_h \cdot u_2)\,(\varepsilon_h \cdot q_1)\,. \tag{2.47}$$

This representation does not limit the generality of our result. If one wishes to consider polarization vectors ε_h, the gauge condition can easily be imposed by sending

$$\varepsilon_h \to \tilde{\varepsilon}_h = \varepsilon_h - \frac{u_1 \cdot \varepsilon_h}{u_1 \cdot k} k\,, \tag{2.48}$$

and evaluating the amplitude using $\tilde{\varepsilon}_s$. In this way, full generality can be restored.

3 Waveform observable from amplitudes

The goal of this work is to compute the waveform emitted during the scattering process of two black holes, where one is rotating, at order $\mathcal{O}(G^3)$ including linear-in-spin effects. For the waveform observable, this is explained through the KMOC formalism [48–50], which relates the waveform to matrix elements including the S-matrix. (See also the recent generalization of such asymptotic observables in ref. [60].)

In the following, we briefly summarize the necessary results to highlight the connection between the gravitational waveform and scattering amplitudes. For more detailed reviews we refer the reader to refs. [50, 56, 59]. Let us start by focusing on the momentum-space waveform observable. It is given by the matrix element $\mathcal{M}^{\vec{s}}$ (and its conjugate)

$$i\hat{\delta}^D(q_1+q_2-k)\mathcal{M}^{\vec{s}}(p_i,q_i,k) = \langle p_1'^{\,s_1'} p_2' |\, S^\dagger a^s(k) S\, |p_1^{s_1} p_2\rangle\,, \tag{3.1}$$

which depends on the spin and helicity quantum numbers of the particles involved in the scattering process, which we collectively denote by $\vec{s} = \{s_1, s_1', s\}$. Furthermore, we absorb some explicit factors of 2π by defining

$$\hat{\delta}^D(x) \equiv (2\pi)^D\, \delta^D(x). \tag{3.2}$$

In order to make contact with the classical scattering of spinning point-like objects, we introduce classical spin variables through a form-factor decomposition [71],

$$\mathcal{M}^{\vec{s}} = \sum_{i=1}^{2}\sum_{j=1}^{4} \mathcal{M}^{ij}\, F_i^s\, T_j^{s_1' s_1}\,, \tag{3.3}$$

using the operator basis (2.37).

The classical spin-dependence of the amplitude $\mathcal{M}^{\vec{s}}$ is obtained by replacing the Pauli-Lubanski spin operator $\mathbb{S}^\mu$ by its classical counterpart S^μ. In terms of the form factor decomposition, the operators T_n are replaced by $T_j^{\rm cl}(S)$ using eq. (2.43),

$$\mathcal{M}^{{\rm cl},s}(S) = \sum_{i=1}^{2}\sum_{n=1}^{4} \mathcal{M}^{ij}\, F_i^s\, T_j^{\rm cl}(S)\Big|_{\rm class}\,, \tag{3.4}$$

where we take the classical scaling limit of the building blocks of the matrix element $\mathcal{M}^{\vec{s}}$ (see section 4). This replacement relies on an observed match between the form-factors of spin-s

JHEP11(2024)109

theories and point-particle theories with classical spin to order $2s$, see ref. [82]. Commonly this relation is coined the *spin universality principle*, which states that the form-factors of spin operators are universal and can be matched between different finite-in spin theories and point particles with continuous spin.[2] For the case at hand, this was verified for the Proca field theory to $\mathcal{O}(G^3)$ and $\mathcal{O}(S^2)$ [71]. A method for dealing with an ambiguity in identifying quadratic-spin terms was recently demonstrated [111]. Here we are concerned with linear-spin terms and leave a computation of the quadratic terms to future work.

We will also consider the spin-less system (2.6) for which the form-factor decomposition only concerns the graviton state. Alternatively, we obtain a matching waveform in the spin system: since the matrix elements are obtained as a polynomial in the spin vector we recover the spin-less waveform for $S^\mu = 0$.

The position-space waveform in the classical limit (2.20) is given by the Fourier transformation [48, 50]. In fact, for large distances from the scattering event, the metric field $h_{\mu\nu}(r)$ admits an expansion in negative powers of $|\mathbf{r}|$. The waveform is identified as the coefficient of the leading-order contribution in this expansion, e.g.

$$h(S, r, p_i, b)\big|_{|\mathbf{r}|\to\infty} = \frac{1}{4\pi|\mathbf{r}|} h^\infty(t - |\mathbf{r}|, S, \mathbf{n}, p_i, b)\,. \tag{3.5}$$

Plugging in $k = \omega\hat{k} = \omega(1, \mathbf{n})$, with $\mathbf{n} = \mathbf{r}/|\mathbf{r}|$, for the graviton momentum and taking the Fourier transform to time-domain and impact parameter space, we have [50]

$$h^\infty(u, S, \mathbf{n}, p_i, b) = \frac{i\kappa}{2}\int_0^\infty \frac{d\omega}{2\pi}\int d^D\mu\, e^{-i\omega u + ib_1\cdot q_1 + ib_2\cdot q_2}\mathcal{M}^{\text{cl},-2}(S, p_i, q_i, k) + \text{c.c.}\,, \tag{3.6}$$

where we define the retarded time $u = t - |\mathbf{r}|$ and introduced the shorthand notation

$$d^D\mu = \left[\prod_{i=1}^{2}\frac{d^Dq_i}{(2\pi)^D}\hat{\delta}(2\bar{m}_i\, u_i\cdot q_i)\right]\hat{\delta}^D(q_1 + q_2 - k)\,. \tag{3.7}$$

We split the impact-parameter vectors into symmetric and anti-symmetric contributions

$$b_1 = b + b_s\,, \quad b_2 = -b + b_s, \tag{3.8}$$

and omit the symmetric one ($b_s = 0$), since it corresponds to a translation of the system, which can be retrieved from a shift in the time variable $t \to (u - b_s\cdot\hat{k})$ in the final observable.

In more conventional notation, the amplitude $h^\infty(u, S, \mathbf{n})$ is related to *plus* and *cross* polarizations of the waveform, which is commonly used in the data analysis of gravitational wave detectors,

$$h_+ = \text{Re}\,[h^\infty + g_0]\,, \qquad h_\times = \text{Im}\,[h^\infty + g_0]\,, \tag{3.9}$$

where g_0 accounts for a constant background of the metric that has to be fixed through initial conditions.

Let us now turn the discussion towards the explicit scattering amplitudes necessary in the computation of the waveform. As eq. (3.1) is already proportional to κ we will need amplitudes

[2] This property has been related to a spin-independence of the three-point amplitude for rotating black holes (see e.g. [76]).

JHEP11(2024)109

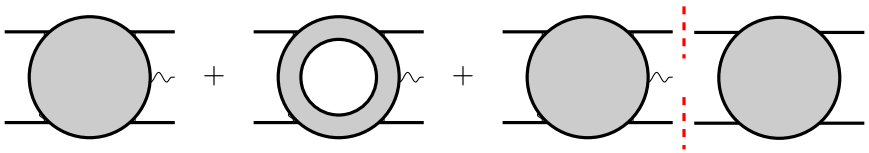

Figure 2. The waveform amplitude is a combination of scattering amplitudes. Up to one loop we require a tree amplitudes, a loop amplitude (the amplitude contribution) and a phase-space integral over a product of tree amplitudes (the cut contribution). We suppress disconnected contributions which do not contribute for generic momenta and frequency.

up to $\mathcal{O}(\kappa^5)$. To this end we express the S-matrix in terms of the transition matrix T, i.e. using $S = 1 + iT$. Plugging in this expansion, we find two contributions to the amplitude [48],

$$\langle p_1'^{s_1'} p_2' | S^\dagger a^s(k) S | p_1^{s_1} p_2 \rangle = i \langle p_1'^{s_1'} p_2' | a^s(k) T | p_1^{s_1} p_2 \rangle + \langle p_1'^{s_1'} p_2' | T^\dagger a^s(k) T | p_1^{s_1} p_2 \rangle, \tag{3.10}$$

with the first one being linear in T and second one quadratic in T. Below we refer to the first term of eq. (3.10) as the *amplitude contribution* and the second we denote the *cut contribution*. The amplitude contribution corresponds to the five-point scattering amplitude $M^{\vec{s}}$,

$$\langle p_1'^{s_1'} p_2' | a^s(k) T | p_1^{s_1} p_2 \rangle = \hat{\delta}^D(p_1' + p_2' + k - p_1 - p_2) M^{\vec{s}}, \tag{3.11}$$

which we need at the tree and one-loop level,

$$M^{\vec{s}} = M^{\text{tree},\vec{s}} + M^{1-\text{loop},\vec{s}} + \mathcal{O}(\kappa^6)\,. \tag{3.12}$$

These contributions are graphically represented by the first two terms of figure 2. The second term, the cut contribution $C^{\vec{s}}$ is given by

$$\langle p_1'^{s_1'} p_2' | T^\dagger a^s(k) T | p_1^{s_1} p_2 \rangle = i \hat{\delta}^D(p_1' + p_2' + k - p_1 - p_2) C^{\vec{s}}, \tag{3.13}$$

which is turned into a phase-space integral of a product of scattering amplitudes by inserting a complete set of states,

$$\langle p_1'^{s_1'} p_2' | T^\dagger a^s(k) T | p_1^{s_1} p_2 \rangle = \sum_n \int d\text{LIPS}_n(\vec{\ell}) \; \langle p_1'^{s_1'} p_2' | T^\dagger | \psi_n^{\vec{p}}(\vec{\ell}) \rangle \; \langle \psi_n^{-\vec{p}}(-\vec{\ell}) | a^s(k) T | p_1^{s_1} p_2 \rangle\,, \tag{3.14}$$

where the sum runs over all n-particle scattering states and the phase-space integration is performed over the respective multi-particle Lorentz-invariant phase space (LIPS). The collection of phase-space momenta and particle polarization labels are denoted by $\vec{\ell} = \{\ell_1, \ldots, \ell_n\}$ and $\vec{p}$, respectively.

The sum over intermediate states simplifies in fixed-order computations. The phase-space integral does not contribute at leading order (for $n = 0, 1$), because of particle flavor conservation, as the two matter lines are associated to distinct particle types. At next-to-leading order, the insertion of two-particle states contribute with two on-shell massive propagators. This contribution corresponds to a two-particle cut and is given by the product of a four-point and a five-point tree,

$$\begin{aligned} \langle p_1'^{s_1'} p_2' | T^\dagger a^s(k) T | p_1^{s_1} p_2 \rangle = \sum_{\hat{s}_1} \int d\Phi_1(\ell_1)\, d\Phi_2(\ell_2)\, \delta^D(\ell_1 + \ell_2 + p_1' + p_2') \\ \times \langle p_1'^{s_1'} p_2' | T^\dagger | \ell_1^{-\hat{s}_1} \ell_2 \rangle \; \langle (-\ell_1)^{\hat{s}_1} (-\ell_2) | a^s(k) T | p_1^{s_1} p_2 \rangle + \mathcal{O}(\kappa^6)\,, \end{aligned} \tag{3.15}$$

JHEP11(2024)109

Figure 3. A one-loop pentagon integral and its two-particle cut. Both, the Feynman integral and the phase-space integral, appear combined in the classical waveform observable.

Here two massive lines appear, that are associated to a vector field and the scalar. This contribution is depicted on the right of figure 2. The corresponding phase-space measures are denoted by $d\Phi_i$ and are defined in eq. (A.10), while $\hat{s}_1$ is the polarization label of the intermediate vector-field. Additionally, there could be contributions coming from disconnected diagrams including three-point trees and propagators. Since we are working with real-valued kinematics, these pieces will only contribute at zero frequency of the emitted graviton. Such a contribution can also be fixed through initial conditions, we do not consider it in this work. Finally, we note that the four-point tree is written in terms of $T^\dagger$ and is therefore evaluated with propagators with the opposite $i\delta$ prescription

$$\frac{1}{p^2 - m^2 + i\delta} \quad \to \quad \frac{1}{p^2 - m^2 - i\delta}, \tag{3.16}$$

as compared to the five-point tree and one-loop amplitudes. We can write the cut contribution as the Cutkosky cut of the one-loop (quantum) amplitude $M^{1-\text{loop},\vec{s}}$ in the $(p_1' + p_2')$-channel, as depicted in figure 3,

$$C^{\vec{s}} \equiv \text{Cut}_{1'2'}\left[M^{1-\text{loop},\vec{s}}\right] . \tag{3.17}$$

The cut contribution plays an important role, by setting causality properties of the total observable [60]. Technically, the cut terms also subtract hyper-classical contributions from the observable [56–58]. With this we have linked the asymptotic observables (3.6) directly to the following scattering data

$$\mathcal{M}^{\vec{s}} = M^{\text{tree},\vec{s}} + M^{1-\text{loop},\vec{s}} + C^{\vec{s}} + \mathcal{O}(\kappa^6) . \tag{3.18}$$

In the next section, we discuss the evaluation of the amplitude functions in the classical limit.

4 Scattering amplitudes computation

We now discuss the computation of the classical scattering amplitudes (3.18). In order to leverage the organizational principle of QFT and exploit established field-theory methods, we perform the computation in two steps: we first compute the quantum scattering amplitudes and then consider their classical limits (2.20).

An important aspect of our computation is that we base it on an exact numerical approach. For the computation of quantum scattering amplitudes we use the program Caravel [89]. At tree level, the program yields numerical results for scattering amplitudes in exact modular arithmetic. At loop level, the program implements the numerical unitarity

JHEP11(2024)109

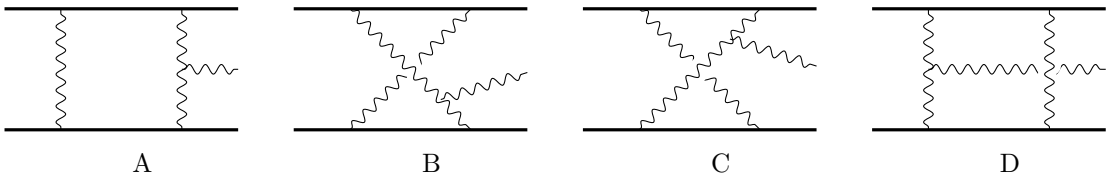

Figure 4. Example Feynman diagrams for the scattering of massive particles interacting through gravitational exchange. Here, wavy lines represent massless gravitons, while solid lines refer to massive scalar or vector-fields.

method [93–97] in the variant of refs. [98–100], which provides numerical values for the rational integral coefficients of a one-loop integral basis. We employ functional reconstruction techniques [101, 102] to obtain analytic expressions for the classical expansions. In order to deal with the classical limit of helicity states, we compute the amplitudes in a form-factor decomposition.

4.1 Organization of the computation

For the computation of the waveform observable we proceed in two steps, we first compute the one-loop amplitude, which admits the standard decomposition,

$$M^{1-\text{loop},\vec{s}} = \sum_{\Gamma\in\Delta} c_\Gamma^{\vec{s}}(\epsilon)\,\mathcal{I}_\Gamma\,, \tag{4.1}$$

where Δ is the set of all one-loop diagrams. Furthermore, $\mathcal{I}_\Gamma$ are the one-loop master integrals and $c_\Gamma^{\vec{s}}(\epsilon)$ the corresponding ϵ dependent integral coefficients. The set of master integrals is a subset of the set of diagrams and we take this into account by allowing vanishing for integral coefficients.

Next we compute the cut in the $(p_1'+p_2')$-channel by recycling the one-loop amplitude computation. The cut of the quantum amplitude in eq. (3.17), is given as a sum of phase-space integrals which is related to cut master-integrals,

$$C^{\vec{s}} = \text{Cut}_{1'2'}\left[\sum_{\Gamma\in\Delta} c_\Gamma^{\vec{s}}(\epsilon)\,\mathcal{I}_\Gamma\right] = \sum_{\Gamma\in\Delta} c_\Gamma^{\vec{s}}(\epsilon)\,\text{Cut}_{1'2'}\left[\mathcal{I}_\Gamma\right]\,, \tag{4.2}$$

where we keep in mind that some of the cuts of the master integrals vanish. The coefficients $c_\Gamma^{\vec{s}}(\epsilon)$ are not affected by cutting and are those of eq. (4.1). Given the similarities between the amplitude and the cut contribution we can combine both via

$$M^{1-\text{loop},\vec{s}} + C^{\vec{s}} = \sum_{\Gamma\in\Delta} c_\Gamma^{\vec{s}}(\epsilon)\,\mathcal{I}_\Gamma^{\text{exp}}\,, \tag{4.3}$$

with the new type of master integrals given by

$$\mathcal{I}_\Gamma^{\text{exp}} \equiv \mathcal{I}_\Gamma + \text{Cut}_{1'2'}\left[\mathcal{I}_\Gamma\right]\,. \tag{4.4}$$

We note that the integrals $\mathcal{I}_\Gamma^{\text{exp}}$ coincide with $\mathcal{I}_\Gamma$ if the cut contribution in the $(p_1'+p_2')$-channel vanishes. In the classical limit, the integrals $\mathcal{I}_\Gamma$ were computed in refs. [56–58] and their

JHEP11(2024)109

generalizations $\mathcal{I}_\Gamma^{\text{exp}}$ in ref. [60]. We have validated the $\mathcal{I}_\Gamma^{\text{exp}}$ integrals and collected our independent computation in appendix B.

Finally, we remark that the cutting procedure of a fixed integral is related to its discontinuity and imaginary part, however, this does not hold true for the classical limit of the full amplitude. In the classical limit, distinct cuts may not be properly resolved which leads to over counting, such that a cut in the (p_1+p_2)-channel is indistinguishable from the one in the $(p_1'+p_2')$-channel, since the difference between the momenta $k = p_1+p_2-(p_1'+p_2')$ is considered to be a sub-leading contribution. Working with a diagrammatic representation of the integrals the association of quantum and classical cuts is manifest and this issue can be avoided.

In summary, we require two types of object, the integrals $\mathcal{I}_\Gamma^{\text{exp}}$ and the coefficients $c_\Gamma^{\vec{s}}(\epsilon)$, both expanded in the classical limit. In the following section 4.2, we discuss the explicit computation of these ingredients within the framework of Numerical Unitarity.

4.2 Brief review of numerical unitarity

For the computation of the amplitudes $M^{\vec{s}}$ we now compute the integral coefficients, $c_\Gamma^{\vec{s}}(\epsilon)$ applying the numerical unitarity method [93–97] in the variant of ref. [98–100]. First, we promote the integral decomposition eq. (4.1) to an integrand decomposition,

$$M^{\vec{s}}(\ell) = \sum_{\Gamma\in\Delta} \sum_{k\in M_\Gamma\cup S_\Gamma} c_{\Gamma,i}^{\vec{s}}(\epsilon)\, \frac{m_{\Gamma,i}(\ell)}{\prod_{j\in P_\Gamma}\rho_j(\ell)} \tag{4.5}$$

where ρ_j denotes the propagator variable. P_Γ denotes the set of propagators associated to diagram Γ. As opposed to the integral decomposition formula in eq. (4.1), the sum in eq. (4.5) runs over integral insertions $m_{\Gamma,i}$ associated to master integrals M_Γ and surface terms S_Γ of a given diagram Γ. While surface terms are necessary to parameterize the integrand, they will ultimately integrate to zero. We construct the surface terms from unitarity compatible integration-by-parts identities [98, 112–114].

The coefficients $c_{\Gamma,i}$ are now obtained by exploiting the factorization property of the loop integrand (4.5). Specifically, we consider loop-momentum values ℓ^Γ where the propagators are on-shell, that is $\rho_j(\ell^\Gamma) = 0$ iff $j \in P_\Gamma$. The leading contribution of the integrand in this limit behaves as

$$\sum_{\vec{s}_i\in\text{states}} \prod_{i\in T_\Gamma} M_i^{\text{tree},\vec{s}_i'}(\ell^\Gamma) = \sum_{\Gamma'\geq\Gamma, i\in M_{\Gamma'}\cup S_{\Gamma'}} c_{\Gamma',i}^{\vec{s}}(\epsilon)\, \frac{m_{\Gamma',i}(\ell^\Gamma)}{\prod_{j\in(P_{\Gamma'}\setminus P_\Gamma)}\rho_j(\ell^\Gamma)}. \tag{4.6}$$

On the left-hand side of this equation, we denote by T_Γ the set of tree amplitudes associated with the vertices in the diagram corresponding to Γ, and the sum is over the states propagating through the internal lines of Γ. On the right-hand side, we sum over integral topologies, denoted by Γ', which contribute to the limit, for which $P_\Gamma \subseteq P_{\Gamma'}$. The coefficients $c_{\Gamma,i}^{\vec{s}}(\epsilon)$ are obtained by solving the system of linear equations given by eq. (4.6) for a sufficient number of values of ℓ^Γ. So far all step were performed numerically. In order to extract the dimensional dependence of the state sums we use the dimension D_s for the Lorentz algebra of the integer-spin particle representations [96]. We vary this parameter over four values, $D_s \in \{5,6,7,8\}$ and extract the coefficients $c_n(\epsilon)$ of the following parameterization

JHEP11(2024)109

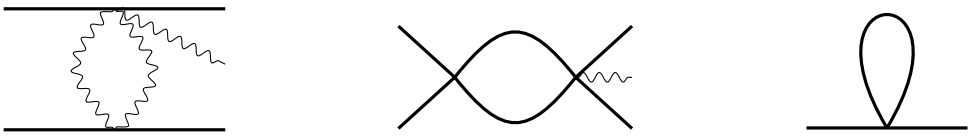

Figure 5. An example of integrals that do not contribute in the classical limit. Anticipating the cancellation the massless bubble contribution is dropped already before we the classical limit. The massive bubble and tadpole integrals turn scaleless and integrates to zero in dimensional regularization in the classical limit.

of the integral coefficients [115],

$$c^{\vec{s}}_{\Gamma,i}(D_s,\epsilon) = \frac{c_0(\epsilon)}{(D_s-2)^2} + \frac{c_1(\epsilon)}{(D_s-2)} + c_2(\epsilon) + c_3(\epsilon)\,(D_s-2). \tag{4.7}$$

This parameterization is set up to capture the explicit D_s dependence of the graviton propagators

$$\frac{i}{p^2+i\delta}\;\frac{1}{2}\left[\eta_{\mu\alpha}\,\eta_{\nu\beta}+\eta_{\mu\beta}\,\eta_{\nu\alpha}-\frac{2}{D_s-2}\eta_{\mu\nu}\,\eta_{\alpha\beta}\right]. \tag{4.8}$$

Similarly, the dependence on the dimensional regulator ϵ is reconstructed from sampling over finite numerical values of ϵ. We evaluate the tree-level scattering amplitudes through Berends-Giele recursion [90] using an implementation of the Feynman rules obtained with the help of xAct [91, 92]. By performing all these calculations using finite-field arithmetic we are able to determine the coefficients exactly as rational functions in ϵ and D_s with no loss of numerical precision. An important technical ingredient for the numerical amplitude computation is a rational parameterization of phase space and the mass parameters. We provide the technical details of this in appendix D.

Having determined the $c^{\vec{s}}_{\Gamma,i}$ as functions in ϵ and D_s at a single numerical phase-space point we obtain the integrated representation (4.1) by dropping surface terms and replacing master integrands, by master integrals. Given that every propagator structure at one loop has at most one associated master integral we suppress the corresponding label and use $c^{\vec{s}}_{\Gamma}$ instead of $c^{\vec{s}}_{\Gamma,1}$.

Finally, we remark, that we simplify the computation by omitting all tadpole integrals and the bubble integral with two massless or two massive propagators. In the unitarity computation, we omit the respective cuts in Δ. The diagrams are displayed in figure 5. Omitting these integrals early is permitted, since they do not contribute in the classical limit, which we anticipate. We explicitly checked on random phase-space points that the bubble diagram does in fact drop out in the classical limit. All massive bubbles and tadpoles reduce to scale-less integrals in the classical limit and vanish in dimensional regularization. It is important to keep the pentagon integrals although they only start contributing at higher orders in ϵ.

4.3 Form-factor decomposition

We now implement a form-factor decomposition of the graviton helicity states and the polarization states of the massive vector field. The motivation is two fold:

JHEP11(2024)109

1. Technically we need good control over the classical scaling limit and the analytic reconstruction, which is achieved by working with the rational form factors instead of polarization states. The decomposition can also impact the compactness of the result. We use gauge-symmetry and scaling considerations in the classical limit to determine the form factors.

2. We intend to relate scattering data of massive vector fields to a spin variable. This step inherently relies on a form-factor decomposition in terms of the Pauli-Lubanski operators introduced in section 2.2.

In our effective field theory, the gravitational wave corresponds to the expectation value of an external graviton and the polarization of the observed wave is related to the polarization tensors $\varepsilon_{\mu\nu}$ of this graviton. For the scattering of four scalar fields and a graviton, we decompose the amplitude in terms of

$$O_i^s = F_i^s\,, \quad i = 1, 2. \tag{4.9}$$

In the presence of vector bosons we instead choose the basis of spin and helicity amplitudes by

$$O_{ij}^{\vec{s}} = F_i^s T_j^{s_1' s_1}\,, \quad i = 1, 2\,, \quad j = 1, \ldots, 9\,, \tag{4.10}$$

and their classical counterparts,

$$O_{ij}^{\mathrm{cl},\vec{s}} = F_i^s T_j^{\mathrm{cl}}\,, \quad i = 1, 2\,, \quad j = 1, \ldots, 9\,, \tag{4.11}$$

using the definition of the graviton monomials (2.47) and the spin decomposition (2.43). We combine them as in eq. (4.10) and consider observables in the decomposition,

$$\mathcal{M}^{\vec{s}} = \sum_n \mathcal{M}^n\, O_n^{\vec{s}}\,, \tag{4.12}$$

where we use the multi-index notation $n = (ij)$ with $i = 1, 2$ and $j = 1, 9$.

For the rational tree amplitudes we have the helicity independent form factors $M^{\mathrm{tree},n}$ according to

$$M^{\mathrm{tree},\vec{s}} = \sum_n M^{\mathrm{tree},n}\, O_n^{\vec{s}}\,. \tag{4.13}$$

By construction, the number of independent spin and helicity configurations, denoted by N=2 (N=18), of the tree amplitude $M^{\mathrm{tree},\vec{s}}$ matches the number of independent tensors $O_n^{\vec{s}}$ of the scalar (2.8) and the scalar-vector (2.9) theory, respectively. Consequently, we extract the scalar form factors directly from 2 (18) helicity amplitudes by solving the linear system

$$\begin{pmatrix} M^{\mathrm{tree},\vec{s}_1} \\ \vdots \\ M^{\mathrm{tree},\vec{s}_N} \end{pmatrix} = \begin{pmatrix} O_1^{\vec{s}_1} & \cdots & O_N^{\vec{s}_1} \\ \vdots & \ddots & \vdots \\ O_1^{\vec{s}_N} & \cdots & O_N^{\vec{s}_N} \end{pmatrix} \begin{pmatrix} M^{\mathrm{tree},1} \\ \vdots \\ M^{\mathrm{tree},N} \end{pmatrix}. \tag{4.14}$$

For the corresponding one-loop amplitudes, we obtain the form factors by decomposing the integral coefficients

$$c_\Gamma^{\vec{s}}(\epsilon) = \sum_n c_\Gamma^n(\epsilon)\, O_n^{\vec{s}}\,, \tag{4.15}$$

JHEP11(2024)109

such that the one-loop amplitude is given by,

$$M^{1-\text{loop},n} = \sum_{\Gamma\in\Delta} c_\Gamma^n(\epsilon)\,\mathcal{I}_\Gamma\,. \tag{4.16}$$

4.4 Classical limit of quantum amplitudes

To realize the classical limit in the quantum scattering amplitudes we follow the procedure outlined below. Due to the different analytical structure of tree-level and one-loop amplitudes we proceed with slightly different strategies.

Our first goal is the analytic reconstruction in the scaling parameter $\bar{m}$, in order to perform the classical expansion. For tree-level amplitudes the classical contributions are given at the order $\bar{m}^4$ (2.23). Using eq. (4.14) allows to obtain the form factors $M^{\text{tree},n}$ for a fixed momentum configuration as

$$M^{\text{tree},n} = \sum_{k=-1}^{1} M_k^{\text{tree},n}(D_s-2)^k\,. \tag{4.17}$$

The coefficients $M_k^{\text{tree},n}$ are rational functions in $\bar{m}$ and we parameterize them as,

$$M_k^{\text{tree},n}(\bar{m}) = \frac{1+\sum_{i=1}^{e_n}\bar{m}^i N_{ki}^n}{\sum_{j=1}^{\tilde{e}_n}\bar{m}^j D_{kj}^n}, \tag{4.18}$$

and compute the parameters N_{ki}^n and D_{ki}^n and the maximal polynomial degrees e_n and $\tilde{e}_n$, from a sufficient number of numerical evaluations of $M_k^{\text{tree},n}$ using Thiele's formula [101, 116]. We then obtain the classical tree amplitude as the leading term in the large-$\bar{m}$ expansion,

$$M^{\text{tree},n}\Big|_{\text{class}} = \bar{m}^4 \sum_{k=-1}^{1} \frac{N_{ke_n}^n}{D_{k\tilde{e}_n}^n}(D_s-2)^k\,. \tag{4.19}$$

As dictated by the limit we kept the highest-order $\bar{m}$-monomials in the numerator and denominator of the rational function $M_k^{\text{tree},n}(\bar{m})$. At this point the ratio $(N_{ke_n}^n/D_{k\tilde{e}_n}^n)$ is a number and we will reconstruct its analytic form using the techniques discussed in the next section.

For the computation it is helpful to understand how the overall mass scaling appears. The graviton form factors F_i, given in eq. (2.47), are homogeneous in $\bar{m}$, so that the mass scaling is manifest in the coefficients $M_k^{\text{tree},n}$. In contrast, the vector-scalar amplitude typically has spurious contributions with $\bar{m}^n$ for $n > 4$, which cancel once the amplitude is combined with the classical form factors containing the spin vectors S^μ. E.g. the proper scaling is easily broken, if the boost factor (2.34) were to be omitted. We have already discussed (see section 2.3) that the subspace transverse to the momentum p, in which the spin is defined, plays a distinguished role in mapping polarization states to a classical spin vector. We attribute the cancellation of unphysical mass scaling to the alignment of frames of the polarization vectors and the spin-tensor decomposition transverse to the frame momentum p. After the expansion of form factors as well as the tensor basis in the classical limit the tree amplitude assumes the expected $\bar{m}^4$ scaling.

JHEP11(2024)109

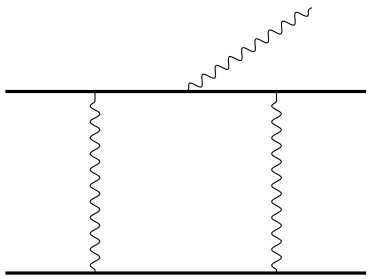

Figure 6. Example pentagon diagram that reduces via partial fractioning to other integral families.

For the one-loop integral coefficients we follow analogous steps to the above and obtain a generalized power series in $\bar{m}$ with rational dependence on D_s and ϵ,

$$c_\Gamma^n(\epsilon, D_s, \bar{m}) = \bar{m}^{p_\Gamma^n} \sum_{k=-2}^{1} \sum_{l=0}^{\infty} c_{\Gamma,kl}^n(\epsilon)(D_s-2)^k \frac{1}{\bar{m}^l} \,. \tag{4.20}$$

with a leading power p_Γ^n in $\bar{m}$ that depends on the integral topology.

We now turn to the computation of the master integrals in the classical limit. For convenience we split the integrals in soft and hard contributions in an expansion by regions [117, 118],

$$\lim_{\bar{m}\to\infty} \mathcal{I}_\Gamma = \mathcal{I}_\Gamma\big|_{\text{eik}} + \mathcal{I}_\Gamma\big|_{\text{hard}} \,. \tag{4.21}$$

The integrals in the hard region are polynomial in the momentum-transfer variables q_i^2 and do not contribute to the long-range observables; they drop out in the Fourier transformation (see section 5.2.3). We thus focus on the eikonal integrals.

The expansion of the scalar integral basis leads to tensor integrals, which we reduce into a basis of eikonal integrals using `LiteRed` [119, 120] and partial fractioning of linearly dependent propagators. An example integral that requires partial fractioning is displayed in figure 6. We obtain the expansion,

$$\mathcal{I}_\Gamma^{\text{exp}}\big|_{\text{eikonal}} = \sum_{\gamma\in\Delta_{\text{eik}}} d_{\Gamma,\gamma}(\epsilon)\, \mathcal{I}_\gamma^{\text{eik}} \,, \qquad d_{\Gamma,\gamma} = \bar{m}^{r_{\Gamma,\gamma}} \sum_{l=0}^{\infty} \frac{1}{\bar{m}^l}\, d_{\Gamma,\gamma}^l(\epsilon) \,. \tag{4.22}$$

where only finitely many expansion terms in $\bar{m}$ are required. Here $\mathcal{I}_\gamma^{\text{eik}}$ is a master-integral basis of eikonal integrals. Δ^{eik} denotes the diagrams associated to the integral basis of eikonal integrals. $r_{\Gamma,\gamma}$ gives the leading scaling of the scalar master integral $\mathcal{I}_\Gamma^{\text{exp}}$ in the classical limit. Combining integrals and coefficients in the $\bar{m}$ expansion, we obtain,

$$\left[M^{1-\text{loop},n} + C^{\vec{n}}\right]\Big|_{\text{class}} = \bar{m}^5 \sum_{k=-2}^{1} \sum_{\gamma\in\Delta^{\text{eik}}} (D_s-2)^k\, c_{\gamma,k}^{\text{eik},n}(\epsilon) \mathcal{I}_\gamma^{\text{eik}} \,, \tag{4.23}$$

where the coefficients $c_{\gamma,k}^{\text{eik},n}$ are suitable linear combinations of the expansions of the integral coefficients (4.20) and the integral reduction (4.22). The individual terms, the one-loop amplitude and the cut contributions have a hyper-classical scaling with $\bar{m}^6$, which drops out in the combination of the terms [56–58, 60].

JHEP11(2024)109

Finally we substitute an expansion of the eikonal master integrals in terms of a functions basis f_i (see appendix B for the definitions) and obtain the classical limit of amplitude and cut contributions

$$\left[M^{1-\text{loop},n} + C^n\right]\Big|_{\text{class}} = \sum_i \left(\frac{r^n_{\text{div},i}}{\epsilon} + r^n_i\right) f_i + \mathcal{O}(\epsilon)\,, \tag{4.24}$$

$$M^{\text{tree},n}\Big|_{\text{class}} = r^n_{\text{tree}} + \mathcal{O}(\epsilon)\,. \tag{4.25}$$

We have used the 't Hooft-Veltman variant of dimensional regularization with $D_s = 4 - 2\epsilon$. Up to now we have discussed how to obtain numerical values for the coefficients r_i for a given set of external moments. Next we will determine their analytic form from sampling over phase-space configurations.

4.5 Analytic reconstruction

We now discuss the computation of the analytic expressions for the rational functions r^n_{tree}, $r^n_{\text{div},i}$ and r^n_i of eq. (4.24), by the functional-reconstruction method [99, 101] in finite-field arithmetic [102].

We start by evaluating the quantum scattering amplitudes on fixed momentum configurations according to eq. (2.10). We generate several sets of external momenta, for every set only a single kinematic invariant of $\{y, \bar{m}_1, \bar{m}_2, \omega_1, \omega_2, q_1^2, q_2^2\}$ is varied. From these univariate functions we can construct a naive ansatz for the rational multivariate functions $\{r^n_{\text{tree}}, r^n_{\text{div},i}, r^n_i\}$ by simply considering the minimal and maximal degree in each variable for the numerator and denominator. This ansatz can be simplified as each multivariate numerator and denominator polynomial has to be homogeneous in the mass dimension. The mass dimensions can be obtained by reconstructing the dependence on t of an univariate slice through all dimensionful parameters, such that

$$(\bar{m}_1, \bar{m}_2, \omega_1, \omega_2) = \vec{a}_1 + \vec{a}_2\, t, \qquad (q_1^2, q_2^2) = \vec{a}_3 + \vec{a}_4\, t + \vec{a}_5\, t^2, \qquad y = a_6 \tag{4.26}$$

where a_i are random numbers. The mass dimension is then given by the maximal degree of t for numerators and denominators. After these steps we now have a rational parameterization of each of the functions r^n_{tree}, r^n_{div} and r^n_i.

We can further simplify the parameterization using the information of the t dependence. The rational coefficients of the pure integral functions f_i, as well as the tree assume the form [121],

$$r^n_i = \frac{\mathcal{N}^n_i}{\prod_j w_j^{q^n_{ij}}} \tag{4.27}$$

where the denominator factors w_i are given by the letters in the symbol alphabet of the integral functions [56–58, 60] (see appendix B) with integer exponents q^n_{ij}. For simplicity we focus on the discussion on the coefficients r^n_i, however, an analogous formula holds for r^n_{tree} and r^n_{div}. The numerators $\mathcal{N}^n_i$ are polynomials in the Lorentz invariants (2.11). The letters that appear in the denominators are collected in eq. (5.20).

JHEP11(2024)109

Knowing the letters w_i we obtain their functional form $w_i(t)$ by evaluating them for the kinematics given in eq. (4.26). Using univariate factorization we can then determine the denominator exponents q_{ij}^n.

All that remains is to determine the numerator polynomials, for which we write a polynomial parameterization. We then set up a system of linear equations for all unknown coefficients and generate sufficient numerical samples of the classical expanded scattering amplitude to obtain solutions. In this way we determine the numerator polynomial with coefficients in a finite field. Finally, we observe that we need two different prime numbers to lift the functional reconstruction of the coefficient functions from the finite-field to the rational numbers. With this we have obtained the analytic form of all functions r_{tree}^n, r_{div}^n and r_i^n for the scalar-scalar and the scalar-vector spectral waveforms.

5 Results

In this section we collect the classical waveform amplitudes $\mathcal{M}^{\vec{s}}$, as given by eq. (3.18), in their leading order and next-to-leading order approximations. Furthermore, we will discuss in depth the analytical properties of the spectral waveforms that we have observed.

5.1 Leading-order amplitudes

The tree-level five-point amplitude for four massive scalar particles and a graviton is given in the supplementary material. The amplitude is given in terms of a form-factor decomposition

$$M^{\text{tree},s} = M_1\, F_1^s + M_2\, F_2^s. \tag{5.1}$$

The scattering amplitude is equivalent to the one obtained in ref. [106], which reads

$$\begin{aligned} M^{\text{tree},s} = -\frac{\kappa^3 \bar{m}_1^2 \bar{m}_2^2}{4}\, \varepsilon_{s,\mu\nu} \Bigg[& \frac{4P^\mu P^\nu}{q_1^2 q_2^2} + \frac{2y}{q_1^2 q_2^2}(Q^\mu P^\nu + P^\mu Q^\nu) \\ & + \left(y^2 - \frac{1}{D_s - 2}\right)\left(\frac{Q^\mu Q^\nu}{q_1^2 q_2^2} - \frac{P^\mu P^\nu}{\omega_1^2 \omega_2^2}\right)\Bigg] , \end{aligned} \tag{5.2}$$

with

$$P^\mu = -\omega_1 u_2^\mu + \omega_2 u_1^\mu , \qquad Q^\mu = (q_1 - q_2)^\mu + \frac{q_1^2}{\omega_1} u_1^\mu - \frac{q_2^2}{\omega_2} u_2^\mu , \tag{5.3}$$

where D_s is the dimensional regularization parameter associated to the spin-degrees of freedom. Furthermore, once linear-in-spin effects are taken into account the scalar-vector tree-level amplitude reads

$$M^{\text{tree},s}(S) = M^{\text{tree},s} + \sum_{i=1}^{2} \sum_{j=2}^{4} M^{\text{tree},ij} F_i^s T_j^{\text{cl}}(S) + \mathcal{O}(S^2) . \tag{5.4}$$

We cross checked the spin tree-amplitude against an independent computation using the worldline quantum field theory formalism matching ref. [51, 52, 122]. The explicit results are given in supplementary material. In particular, in the $S^\mu \to 0$ limit, we recover the tree amplitude of the scalar-scalar scattering.

JHEP11(2024)109

5.2 Next-to-leading order waveform

At the one-loop level we divide the waveform amplitude into its tree-level part and a part that is infrared (IR) divergent, one that is ultraviolet (UV) divergent, a tail, and finite contributions. Thus, the bare waveform amplitude reads

$$\mathcal{M} = M^{\text{tree}} + \mathcal{M}^{\text{IR}} + \mathcal{M}^{\text{UV}} + \mathcal{M}^{\text{tail}} + \mathcal{M}^{\text{finite}} + \mathcal{O}(\epsilon)\,, \tag{5.5}$$

where we drop terms of order ϵ. Let us comment briefly on the individual terms. The tree contribution is identical to the one presented in section 5.1. Next, the IR divergent terms are a phase and can be absorbed into a redefinition of the coordinate time in the position-space waveform as shown below. The term is explicitly given by

$$\mathcal{M}^{\text{IR}} = \left[\frac{1}{\epsilon} - \log\left(\frac{\mu_{\text{IR}}^2}{\mu^2}\right)\right] \mathcal{W}_S\, M^{\text{tree}}. \tag{5.6}$$

The soft factor of the waveform $\mathcal{W}_S$ is discussed below in section 5.2.2. A derivation of $\mathcal{W}_S$ can be found in appendix C. Furthermore, the UV divergent contributions are given by

$$\mathcal{M}^{\text{UV}} = \left[\frac{1}{\epsilon} - \log\left(\frac{\mu_{\text{UV}}^2}{\mu^2}\right)\right] \overline{\mathcal{M}}^{\text{UV}}, \tag{5.7}$$

where $\overline{\mathcal{M}}^{UV}$ is local in momentum-transfer variables q_1 and q_2. Consequently they yield local contribution in impact-parameter space and drop out of the far-field waveform. The tail and finite terms combine to give the characteristic waveform patterns of gravitational scattering processes. The tail contribution is given by

$$\mathcal{M}^{\text{tail}} = -\log\left(\frac{\omega_1\omega_2}{\mu_{\text{IR}}^2}\right) \mathcal{W}_S\, M^{\text{tree}} - \log\left(\frac{\omega_1\omega_2}{\mu_{\text{UV}}^2}\right) \overline{\mathcal{M}}^{\text{UV}}\,, \tag{5.8}$$

while the finite remainder is defined through

$$\mathcal{M}^{\text{finite}} = \sum_{i=1}^{18} f_i r_i\,, \tag{5.9}$$

with the functions f_i given in eq. (B.34). We provide supplementary material containing the waveform observable at $\mathcal{O}(G^3)$ up to linear in spin corrections. The folder structure is as follows:

```
anc/waveform.m

anc/loadWaveform.wl
```

The file `waveform.m` contains the LO (G^2) and NLO (G^3) waveforms with and without spin. The spin dependence is given in terms of the form-factor decomposition in eq. (2.43). The notebook `loadWaveform.wl` contains the notation and commands to load and utilize the waveforms.

JHEP11(2024)109

5.2.1 Waveform for two spinning objects

We have computed the scattering of a vector boson and a scalar and focus on linear in spin corrections for one black hole. At this order, the spin corrections for the second black hole can be obtained from symmetrization. However, some care is required due to the gauge condition $u_1 \cdot \varepsilon_h = 0$. A naive symmetrization would lead to expressions with two gauge conventions. First one needs to remove this gauge condition by the replacement $\varepsilon_h \to \tilde{\varepsilon}_h$ (2.48), after which symmetrization can be done consistently.

5.2.2 Infrared singularities

Both contributions, the amplitude and its cut, develop IR divergences. In ref. [103] it has been shown that the IR pole factorizes into a *soft factor* and the tree-level amplitude. The divergence is related to soft gravitons being exchanged between all pairs of external particles. The same logic applies to the cut amplitude, but now only graviton exchanges that are consistent with the cut topology in figure 3 are taken into account. We review the soft factors for the amplitude and the cut contributions in appendix C. This leads to a subtraction of the super-classical contributions in the soft factor of the complete waveform amplitude $\mathcal{M}$ and additionally alters the classical piece. The combined IR pole is given by [60],

$$\mathcal{M}|_{\text{IR}} = \frac{1}{\epsilon}\mathcal{W}_S\, M^{\text{tree}}, \quad \text{with} \quad \mathcal{W}_S = iG(\bar{m}_1\omega_1 + \bar{m}_2\omega_2)\left(1 + \frac{y(2y^2-3)}{2(y^2-1)^{3/2}}\right). \tag{5.10}$$

Here we suppress spin and helicity labels, since the same relation holds for the scalar-scalar as well as the vector-scalar scattering process.

The result exponentiates into a total phase and can safely be absorbed into an infinite redefinition of the retarded time u, more precisely,

$$e^{-i\omega u}\mathcal{M} \;=\; e^{-i\omega\left[u-\left(\frac{1}{\epsilon}-\log\frac{\mu_{\text{IR}}^2}{\mu^2}\right)\frac{\mathcal{W}_S}{\omega}\right]}\left(M^{\text{tree}} + \mathcal{M}^{\text{UV}} + \mathcal{M}^{\text{tail}} + \mathcal{M}^{\text{finite}}\right) + \mathcal{O}(G^3)\,. \tag{5.11}$$

In fact, this redefinition has an interpretation in classical general relativity. The term,

$$\Delta u_{\text{out}} = \frac{2G}{\omega}(\bar{m}_1\omega_1 + \bar{m}_2\omega_2)\log\left(\frac{r_{\text{obs}}}{r_{\text{min}}}\right), \tag{5.12}$$

corresponds to the Shapiro delay [123], where r_{min} is the distance at closest approach and r_{obs} is the distance of the observer. It is interpreted as the time delay a graviton experiences when escaping the gravitational potential of the massive bodies, as was already pointed out in ref. [57]. The cut contribution gives rise to an additional time-delay (or advance),

$$\Delta u_{\text{in}} = \frac{2G}{\omega}(\bar{m}_1\omega_1 + \bar{m}_2\omega_2)\frac{y(2y^2-3)}{2(y^2-1)^{3/2}}\log\left(\frac{r_{\text{in}}}{r_{\text{min}}}\right), \tag{5.13}$$

where r_{in} is the initial distance between the two black holes. This result was obtained in a classical analysis [60] by integrating along a geodesic in Schwarzschild spacetime from infinity to closest approach. It thus originates from the deflection of the trajectory of an incoming particle due to general relativistic effects. We have verified that the classical derivation also holds in a Kerr space time and that the time delay is equivalent for spinning and non-spinning black holes, as is also predicted by Weinberg's theorem. Geometrically, this is due to the suppression of the angular momentum terms in the Kerr metric at large radial distance.

JHEP11(2024)109

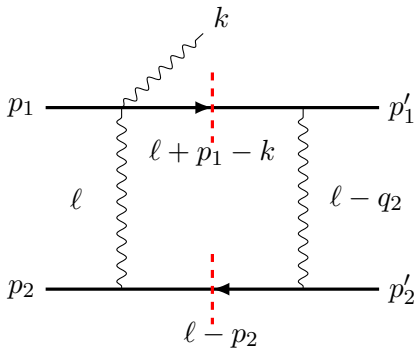

Figure 7. A box cut that is part of the cut contribution. The momenta $\{p_1, p_2\}$ are incoming, $\{p_1', p_2', k\}$ outgoing and ℓ flows clockwise in the diagram.

5.2.3 Ultraviolet singularities

Apart from the soft divergence predicted by Weinberg's theorem there is an additional ϵ pole $\mathcal{M}^{\text{UV}}$ coming from the cut of the amplitude. For the scalar expectation value it is proportional to,

$$\mathcal{M}\big|_{\text{UV}} = -\left(\frac{\kappa}{2}\right)^5 \frac{i}{8\pi\epsilon}(\bar{m}_1\omega_1 + \bar{m}_2\omega_2)\frac{\bar{m}_1^2\bar{m}_2^2(\omega_1^2+\omega_2^2+y\omega_1\omega_2)(1-2y^2)^2}{\omega_1\omega_2^3(y^2-1)^{3/2}}\, F_1^{2h}\,. \tag{5.14}$$

The pole does not correspond to a UV divergence of the quantum amplitude but is instead introduced by the eikonal expansion. To discuss the origin of the additional UV divergence in the eikonal integrals, we consider the box integral figure 7,

$$\mathcal{I}_{\text{box}} = \int \frac{d^D\ell}{(2\pi)^D}\frac{1}{\ell^2\,[(\ell+p_1-k)^2-m_1^2](\ell-q_2)^2[(\ell-p_2)^2-m_2^2]}\,, \tag{5.15}$$

where it is understood that all propagators carry an additional $+i\delta$. In the $\bar{m}\to\infty$ limit the integrals appearing in our calculation are split into eikonal ($\ell\sim\bar{m}^0$) and hard region ($\ell\sim\bar{m}^1$) integrals (see eq. (4.21)). The expansion of the second massive propagator in these regions is given by

$$\frac{1}{(\ell-p_2)^2-m_2^2+i\delta} = \begin{cases} \frac{1}{-2\bar{m}_2u_2\cdot\ell+i\delta} - \frac{\ell\cdot(\ell-q_2)}{[-2\bar{m}_2u_2\cdot\ell+i\delta]^2} + \dots & \text{(eikonal)}\,, \\ \frac{1}{(\ell-\bar{m}_2u_2)^2-\bar{m}_2^2+i\delta} + \frac{\ell\cdot q_2}{[(\ell-\bar{m}_2u_2)^2-\bar{m}_2^2+i\delta]^2} + \dots & \text{(hard)}\,. \end{cases} \tag{5.16}$$

Similar expressions hold for the expansion of the second massive propagator. The singular behavior of the expanded integrals is related to the original unexpanded integral, but may differ in an important way. While the eikonal (hard) expansion matches the IR (UV) behavior of the unexpanded integral, additional divergences develop in the UV (IR) of the eikonal (hard) expansion. These additional divergences have to cancel between the eikonal and the hard region since there is no corresponding divergence in the original integral.

The appearance of UV singularities in the eikonal integral is seen from the expansion of the massive propagators. The leading term in the eikonal expansion scales as $1/\ell$ in the UV limit ($\ell\to\infty$), however, each additional expansion order increases the scaling degree by one. It follows that even if an unexpanded integral containing massive propagators is UV finite,

JHEP11(2024)109

additional UV divergences will be introduced at some order of its eikonal expansion. Whether a UV divergence does in fact appear depends on the expansion order. For the integral at hand we require an eikonal expansion to order $\bar{m}^{-4}$, which is UV divergent.

In our computation, UV contributions appear in intermediate stages of the computation in the classical limit. They can be seen to cancel in the one-loop amplitude, which produces a $1/\epsilon$ pole that matches the universal IR factorization [103]. In contrast, we do observe a non-vanishing UV contribution from the cut contribution, defined in eq. (3.17). We have verified this in two ways:

1. We have compared the $1/\epsilon$ pole of the cut contribution to Weinberg's soft theorem and found a mismatch. To this end we adjusted Weinberg's theorem to the waveform computation (see appendix C).

2. We explicitly computed the UV pole of the cut. This was done by adding a regulator mass $\mu_{\rm IR}^2$ into the quadratic propagators before evaluating the cut of the eikonal expansion in the UV limit. For the above example $\mathcal{I}_{D,\rm box}$ (5.15) this amounts to,

$$\frac{1}{\ell^2 - \mu_{\rm IR}^2 + i\delta}\,, \qquad \frac{1}{(\ell - q_2)^2 - \mu_{\rm IR}^2 + i\delta}\,. \tag{5.17}$$

   The mass regulates the IR singularities, so that the full $1/\epsilon$ pole can be associated to the UV. This computation produced the difference of the $1/\epsilon$ pole of the cut contribution compared to Weinberg's infrared theorem [103].

Finally, we observe that the UV contribution has the expected analytic properties. In fact the UV contribution of the eikonal region lies in the intersection of the hard and the eikonal functions; since the two must cancel. It thus has analytic properties of the hard and the eikonal contributions, i.e. it is polynomial in the momentum-transfer variables q_i. We observe this property in eq. (5.14) and the analogous expression for the spin waveform.

We end this section with a remark about the phase space of the two-particle cut. This phase space is compact for the quantum amplitude, namely a two-dimensional sphere in four dimensions determined by the zero set of the quadratic polynomials,

$$(\ell + p_1 - k)^2 - m_1^2 = (\ell - p_2)^2 - m_2^2 = 0\,. \tag{5.18}$$

Consequently, there is no large-momentum region associated to this cut. This is in contrast to the two-particle cut in the eikonal limit, where two eikonal propagators are forced onto their mass shell,

$$u_2 \cdot \ell = u_2 \cdot \ell = 0\,. \tag{5.19}$$

These on-shell conditions are linear, such that the resulting phase-space integral is performed over a two-dimensional plane, which is non-compact. The boundary of this phase space is then a large momentum region attributed to the UV. This argument supports the surprising fact that the cut contribution does yield a UV divergence.

JHEP11(2024)109

5.3 Analytic properties

The rational coefficients of the pure integral functions f_i, as well as the tree take a particular form (5.20), which has interesting physics implications. We observe that the following letters

$$\begin{aligned}\{w_i\}_{i=1,15} = \Big\{&\omega_1, \omega_2, q_1^2, q_2^2, y+1, y-1, \omega_2^2 - q_1^2, \omega_1^2 - q_2^2,\\ &\omega_1^2 + q_2^2(y^2-1), \omega_2^2 + q_1^2(y^2-1), \omega_1^2 - 2\omega_1\omega_2 y + \omega_2^2,\\ &4\omega_2^2 q_2^2 + (q_1^2 - q_2^2)^2, 4\omega_1^2 q_1^2 + (q_1^2 - q_2^2)^2,\\ &\omega_1^2 q_1^4 - 2\omega_1\omega_2\, q_1^2 q_2^2 y + \omega_2^2 q_2^4,\\ &4\omega_1^2(\omega_2^2 - q_1^2) + 4\omega_1\omega_2 y(q_1^2 + q_2^2) - 4\omega_2^2 q_2^2 + (y^2-1)(q_1^2 - q_2^2)^2\Big\}\end{aligned} \tag{5.20}$$

appear in the denominators, where w_9, w_{10}, w_{14} and w_{15} are absent in the scalar waveform. Most of the 15 letters are related to Gram determinants. We note that, in addition to the integral reduction, the form-factor decomposition introduces Gram determinants in the denominator. The latter denominators cancel when transverse spin vectors and polarization states for the graviton are introduced. To be concrete, we find that (up to overall numerical factors)

$$\{w_7, w_8\} \sim \Big\{G(q_1, u_2),\, G(q_2, u_1)\Big\}, \tag{5.21}$$

as well as

$$\begin{aligned}\{w_9, \ldots, w_{13}\} \sim \Big\{&G(u_1, u_2, q_2),\, G(u_1, u_2, q_1),\\ &G(u_1, u_2, q_1+q_2),\, G(u_2, q_1, q_2),\, G(u_1, q_1, q_2)\Big\},\end{aligned} \tag{5.22}$$

and finally

$$w_{15} \sim G(u_1, u_2, q_1, q_2). \tag{5.23}$$

Note that $G(u_1, u_2, q_1, q_2)$ is equivalent to tr_5^2, where

$$\mathrm{tr}_5 = 4i\, \epsilon_{\mu\nu\alpha\beta}\, u_1^\mu u_2^\nu q_1^\alpha q_2^\beta. \tag{5.24}$$

Therefore, the appearance of w_{15} in the denominators corresponds directly to a double pole. At last, we want to remark that w_{14} is related to the modified Cayley determinant (see e.g. ref. [124]) of the linearized pentagon integral.

The form (4.27) has interesting physical implications: first of all, the mass parameters do not appear in the function alphabet. Consequently they appear in polynomial form through $\mathcal{N}_i^n$, as observed in ref. [125, 126]. Second, the rational form of the coefficients implies that the waveform at fixed-order is determined by a finite set of polynomial coefficients of the numerator and denominator functions $\mathcal{N}_i^n$ and w_i. Finally, in a further expansion, such as a PN expansion, the expansion of the denominator letters imply repetitive patterns. In light of that, only a finite number of terms is required to obtain the full PM expansion, provided the integral functions and the function alphabet is known.

In order to simplify our expressions, we exploit the observation that partial fractioned coefficients r_i^n take a simple form, with reduced mass dimension of numerator and denominator. We use the algorithm [127] (see also [128]) based on polynomial division to obtain compact analytic forms of the waveform functions.

JHEP11(2024)109

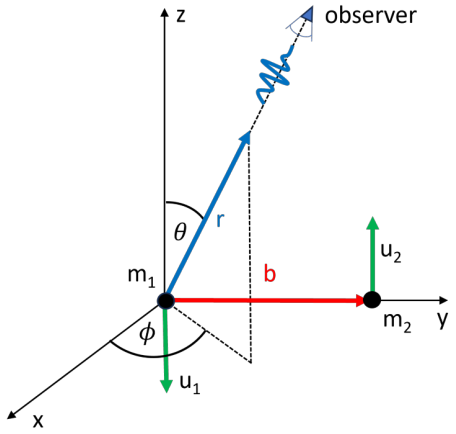

Figure 8. Parameters and coordinate system for observer of radiation from two-object scattering process.

6 Fourier transformation

In order to make contact with a signal that could be observed in a gravitational wave detector, we must perform the Fourier transformation to time-domain and impact-parameter space given in eq. (3.6). After absorbing the IR divergences into the redefinition of the retarded time, we are left with the integral

$$h^{\infty} = \frac{i\kappa}{2}\int_0^{\infty}\frac{d\omega}{2\pi}\int d^D\mu\, e^{-i\omega u+ib\cdot q_1}\left(M^{-2}_{\text{tree}}+\mathcal{M}^{-2}_{\text{finite}}+\mathcal{M}^{-2}_{\text{tail}}+\mathcal{M}^{-2}_{\text{UV}}+\text{c.c.}\right). \tag{6.1}$$

The UV divergent contribution is polynomial in q_i and integrates to $\delta(|b|)$ in the Fourier transformation, being at the same time associated to the hard region (4.21). Since such terms do not contribute to the far-field waveform, we drop the UV contribution from now on. The tree, the finite one-loop waveform and the tail term yield finite results.

We start by defining a reference frame and initial conditions for the external kinematics. We choose the frame shown in figure 8 where the position of the observer is given in terms of Euler angles. Hence, the graviton momentum and the (-2)-polarization are

$$k^{\mu} = \omega\begin{pmatrix}1\\ \cos\phi\sin\theta\\ \sin\phi\sin\theta\\ \cos\theta\end{pmatrix}, \quad \varepsilon^{\mu\nu}_{-2} = \varepsilon^{\mu}_{-}\varepsilon^{\nu}_{-} \quad \text{with} \quad \varepsilon^{\mu}_{-} = \frac{1}{\sqrt{2}}\begin{pmatrix}0\\ \cos\phi\cos\theta+i\sin\phi\\ \cos\theta\sin\phi-i\cos\phi\\ -\sin\theta\end{pmatrix}. \tag{6.2}$$

As suggested by ref. [61], we define the external states and their initial separation to be with respect to u_1 and u_2,

$$u_1^{\mu} = (\gamma,\,0,\,0,\,-\sqrt{\gamma^2-1}), \quad u_2^{\mu} = (\gamma,\,0,\,0,\,\sqrt{\gamma^2-1}), \quad b^{\mu} = (0,\,|b|,\,0,\,0). \tag{6.3}$$

Since γ corresponds to the Lorentz factor it is related to the initial velocity $\pm v$ of each of the black holes through $\gamma = 1/\sqrt{1-v^2}$. We will show plots of waveforms for the observer at position $\phi = 7\pi/10$, $\theta = 7\pi/5$ and a range of initial velocities. All plots are for an equal mass

JHEP11(2024)109

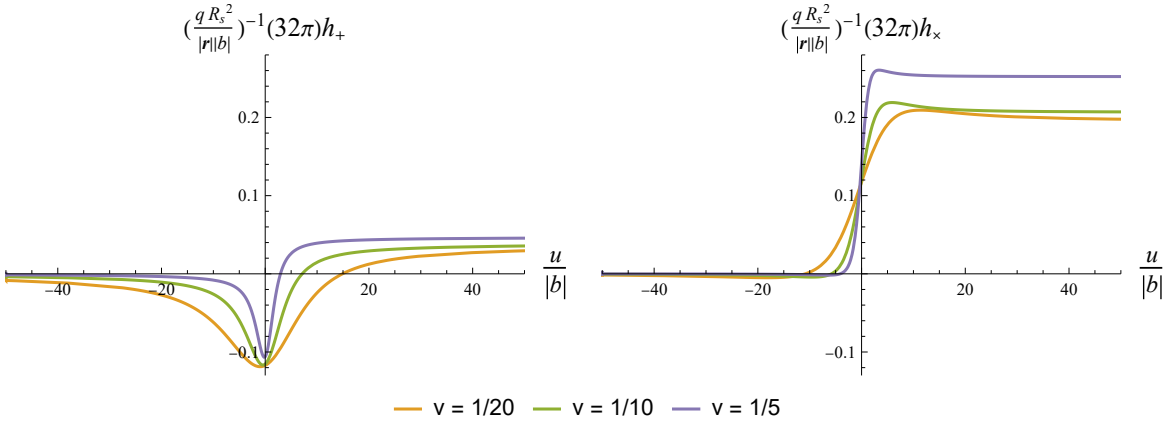

Figure 9. The leading-order waveform emitted during the scattering of two Schwarzschild black holes.

black hole binary, i.e. $q = 1$, with $m_1 = m_2 = M_\odot$. Typical LIGO-Virgo-KAGRA source waveforms with $m_i \sim 30M_\odot$ would only differ by an overall scale from what we present. Note that the difference between m_i and $\bar{m}_i$ is subsubleading in the classical expansion and we hence neglect it in the Fourier transformation. We now turn our attention to the actual integration in eq. (6.1). First, q_2 is integrated out using the delta-function enforcing energy-momentum conservation. Next, q_1 is parameterized by

$$q_1^\mu = z_1 u_1^\mu + z_2 u_2^\mu + z_b \frac{b^\mu}{|b|} + z_v \frac{v^\mu}{|v|} \quad \text{with} \quad v^\mu = \epsilon^{\mu\nu\rho\sigma} u_{1\nu} u_{2\rho} b_\sigma \,, \tag{6.4}$$

which introduces an overall Jacobi-factor of $1/\sqrt{y^2-1}$. The integral over z_1 and z_2 can be evaluated by solving the two constraints given in the delta functions introduced by the on-shell conditions. The problem is hence reduced to the integration over the three variables z_b, z_v and ω. For these final steps, we follow the semi-analytical approach outlined in ref. [56]. In the following, we focus on the calculation of the different pieces in eq. (6.1). As a final point, we note that there could be a non-dynamical background contributing to the waveform, since we have been consistently neglecting zero frequency ($\omega = 0$) terms. Luckily, a gravitational wave detector only measures the changes in the curvature of space-time. We hence 'gauge' our signal by subtracting the value at $u/|b| = -300$.

The Fourier transformation of the tree can be performed fully analytical with the use of the residue theorem. Additionally, poles at infinity are regularized using a principle value prescription [83]. We show results for two Schwarzschild black holes in figure 9 for an observer at $\phi = 7\pi/10$, $\theta = 7\pi/5$.

The one-loop waveform $\mathcal{M}^{\text{finite}}$ contains functions, such as square-roots and logarithms, not present at tree level, which complicates the task significantly. As explained in detail in ref. [56], the integration over ω naturally splits the waveform into two pieces, where one can be written as derivatives of a principle value $\text{PV}(\frac{1}{u/|b|+z_b})$ and the other as derivatives of a delta function $\delta(u/|b| + z_b)$. This allows for an analytic integration of z_b using residues. The numerical integration over z_v is stable for the scalar waveform. When discarding the cut-contribution, we reproduce figure (11) of ref. [56]. Adding the cut amplitude changes the

JHEP11(2024)109

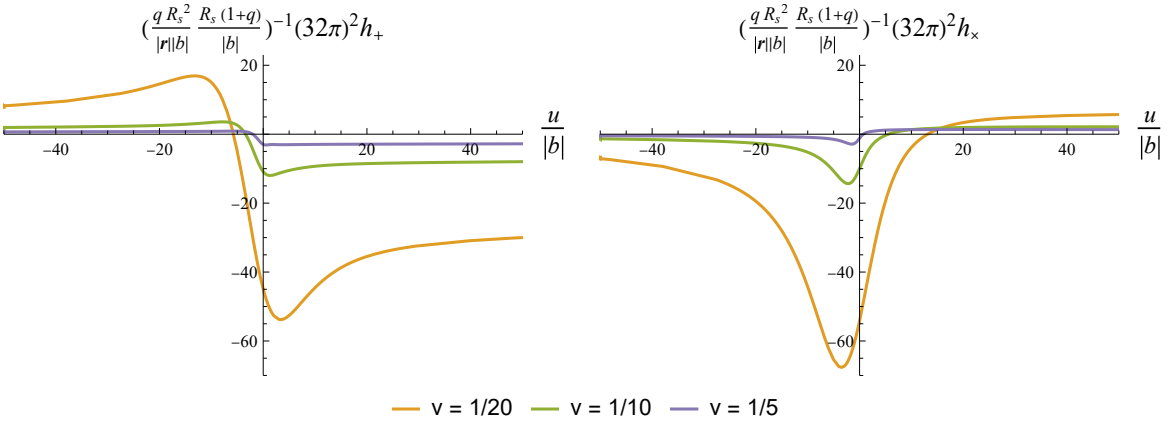

Figure 10. The next-to-leading order correction to the waveform emitted during the scattering of two Schwarzschild black holes. The scale-dependent tail contribution is omitted.

waveform and results are displayed for a range of velocities at position $\phi = 7\pi/10$, $\theta = 7\pi/5$ in figure 10. (Explicitly, we show the finite part of the waveform, $\mathcal{M}^{\text{finite}}$, with the normalization factor $c_N|_{\epsilon=0}$ (B.33) evaluated in four dimensions. The explicit formula for $\mathcal{M}^{\text{finite}}$ is given in the supplementary material.) We note, that the choice made on how to separate the tail from the finite piece significantly influences this result.

The spin corrected waveform introduces additional challenges for the stable numerical integration over z_v after following the outlined steps. We hence leave this Fourier transformation to future work.

7 Validation

Let us summarize in this section the cross checks that we have performed on our computations.

Amplitude Computation: the numerical computation of the integral coefficients $c^{\vec{s}}_{\Gamma,i}(\epsilon)$ is performed using the well-tested Caravel framework. The necessary tree-level scattering amplitudes involved in the unitarity cut computations have been already used at the two-loop level [71], which yields strong consistency checks of the amplitudes. For every phase-space point we perform the so-called $N = N$ check, i.e. we determine the coefficients $c^{\vec{s}}_{\Gamma,i}(\epsilon)$ by sampling eq. (4.6) sufficiently often. Afterwards, we generate an additional on-shell loop-momentum configuration ℓ^Γ and compute both sides of eq. (4.6) to check if the integrand parameterization spans the entire amplitude.

Master Integrals: we computed independently all necessary master integrals and their corresponding cut. We extracted analytical expressions from high-precision evaluations using AMFlow [129], which we validated against pySecDec [130]. Furthermore, we found perfect agreement with ref. [60] after translating conventions.

Analytical Reconstruction: the analytically reconstructed amplitude expressions are validated by numerical means. We evaluate them at a phase-space point in a finite-field for a cardinality that was not used in the reconstruction and compare the results with a

JHEP11(2024)109

direct numerical computation within CARAVEL using the same cardinality. Furthermore, we checked that the classical expanded amplitude is independent of the choice of basis for the intermediate form-factor decomposition by changing the tensors in eq. (2.37).

Spectral Waveform: for tree-level scalar-scalar scattering we reproduce the result of ref. [106], while the scalar-vector tree-level amplitude is validated against an independent computation using the worldline quantum field theory formalism. We also reproduce the results of ref. [52]. The one-loop building block for the scalar-scalar scattering has been validated against previous results of refs. [56, 57]. Furthermore, we also find agreement with the independent computations [131, 132] for the cut contribution including the presence of additional UV divergences and with [133] up to q_i-independent terms and an overall factor i. Finally, for both, scalar-scalar and scalar-vector, the infrared divergences of the combined amplitude and cut contributions agree with Weinberg's infrared factorization formula [103]. In addition, we verified that the scalar-vector amplitude reduces to the scalar-scalar one in the limit $S \to 0$. Finally, we compared the loop-level spectral waveform to an independent computation using a worldline quantum-field-theory [52] in the in-in formalism [134], where the metrix-fluctuation appears as classical expectation value. In this comparison we used the integrals [60] with Feynman-$i\epsilon$ prescriptions for gravitons, as opposed to retarded ones.

Fourier Tranformation: we confirm the cancellation of all unphysical poles in the spectral waveform. We perform this check by analyzing the vanishing locus of the denominator factors of eq. (5.20) on the physical phase space. That is, we evaluate the spectral waveform, see eq. (3.6), for fixed helicity and spin assignment on generic lines through the vanishing loci and numerically confirm that the functions are smooth. Ignoring the cut contribution we also reproduce figure (11) of ref. [56].

8 Conclusion

We computed the gravitational Bremsstrahlung to next-to-leading order, i.e at $\mathcal{O}(G^3)$ in the gravitational coupling expansion in the weak field regime. We also compute for the first time linear-in-spin (S^μ) effects. To formulate the classical observable we study the time dependent expectation value of the metric fluctuation, which is interpreted as the waveform of the emitted gravitational wave. To organize the computation we embed the system into minimally coupled second-quantized field theories, which we consider in a scaling limit, associated to the classical point-particle dynamics. The results extend recent computations of the same observable [56–58], including cut contributions [60, 131–133] and spin terms.

We consider two types of theories. Two distinct massive scalar theories, which yield the dynamics of spin-less black-hole scattering. To describe the scattering of a spinning and a spin-less black hole, we use the minimally coupled scalar theory, as well as minimally coupled massive vector fields (Proca theory). In this setup one can obtain up to quadratic in spin corrections [71, 82], and we focused here on the linear term.

The classical observable is obtained from tree-level and one-loop scattering amplitudes and its two-particle cut in the eikonal limit. The results validate a generalization of the

JHEP11(2024)109

universal IR factorization formula of Weinberg and a recent prediction for the IR of the classical waveform observable [60]. Surprisingly, we encounter as well a UV divergence in intermediate steps. The UV divergence is associate to the overlap of the eikonal and hard region of the Feynman integrals in their classical limit. The divergence is local in the momentum transfer and drops out after Fourier transformation to impact parameter space in the far field. In this context we also point out another surprising feature of the classical limit, namely that UV singularities can be obtained in one-loop cuts.

We observe interesting analytic properties in the spectral waveform. The coefficients of the transcendental and algebraic basis functions are rational expressions, whose denominators are symbol letters of the functions characteristic alphabet of the basis of integral functions. We anticipate that this property leads to repeated patterns in further expansions of the present post-Minkowskian result, e.g. in the post-Newtonian limit.

For the computation of scattering amplitudes, we applied the numerical unitarity approach in combination with analytic reconstruction. In order to find compact final expressions, we used partial-fraction decomposition based on methods in algebraic geometry. Within this setup we anticipate that higher-spin corrections are well within reach in the near future. Finally, we are looking forward to further developments towards the computation of higher-order gravitational corrections and the advancement of multi-loop integration techniques and the classical waveform observable.

Acknowledgments

We gratefully acknowledge collaboration with Fernando Febres Cordero on the implementation of one-loop unitarity cuts in the Caravel program. We particularly thank Henrik Johansson and Lucile Cangemi for many discussions and hospitality at NORDITA. We would like to thank Andreas Brandhuber, Graham Brown, Gang Chen, Stefano De Angelis, Joshua Gowdy, Gabriele Travaglini, Alessandro Georgoudis, Carlo Heissenberg, Ingrid Vazquez-Holm for very helpful discussions and the comparison of the scalar spectral waveform. We are particularly grateful to Radu Roiban and Fei Teng for discussions and their cross-checks for the scalar results. We thank Samuel Abreu, Vittorio Del Duca, Paolo Di Vecchia, Riccardo Gonzo, Sara Gündogdu, Enrico Herrmann, Lucio Mayer, Donal O'Connell, Paolo Pichini, Jan Plefka, Rafael Porto, Michael Ruf, Rudolfo Russo, Chia-Hsien Shen, Jan Steinhoff, Mao Zeng for discussions. LB acknowledges support from the Swiss National Science Foundation (SNSF) under the grant 200020 192092. LB acknowledges NORDITA for generously hosting them during the three-month Visiting PhD Fellow Program. M.K. is supported by the DGAPA-PAPIIT grant IA102224 at UNAM. The authors acknowledge the Instituto de Física (UNAM) for providing computing infrastructure and Carlos Ernesto López Natarén for his HPC support.

A Field theory

The Einstein-Hilbert Lagrangian $\mathcal{L}_{\rm EH}$ is given by,

$$\mathcal{L}_{\rm EH} = -\frac{2}{\kappa^2}\sqrt{|g|}R\,, \tag{A.1}$$

JHEP11(2024)109

where $g = \det(g_{\mu\nu})$ and R the Ricci scalar contraction $R = R^{\rho}{}_{\mu\rho\nu}\, g^{\mu\nu}$ of the Riemann tensor. We use the conventions,

$$R^{\mu}{}_{\nu\rho\sigma} = \partial_\rho \Gamma^{\mu}{}_{\nu\sigma} - \partial_\sigma \Gamma^{\mu}{}_{\nu\rho} + \Gamma^{\mu}{}_{\alpha\rho}\Gamma^{\alpha}{}_{\nu\sigma} - \Gamma^{\mu}{}_{\alpha\sigma}\Gamma^{\alpha}{}_{\nu\rho}\,, \tag{A.2}$$

$$\Gamma^{\mu}{}_{\nu\rho} = \frac{1}{2} g^{\mu\sigma}\left[\partial_\nu g_{\sigma\rho} + \partial_\rho g_{\sigma\nu} - \partial_\sigma g_{\nu\rho}\right]. \tag{A.3}$$

The linearized Riemann tensor is given by,

$$R_{\mu\nu\rho\sigma} = -\frac{\kappa}{2}[\partial_\mu\partial_\rho h_{\nu\sigma} - \partial_\mu\partial_\sigma h_{\nu\rho} - \partial_\nu\partial_\rho h_{\mu\sigma} + \partial_\nu\partial_\sigma h_{\mu\rho}]. \tag{A.4}$$

In order to clarify our conventions, we introduce quantum fields and state spaces next. The graviton operator can be expanded in its modes as

$$\eqsim_{\mu\nu}(r) = \sum_{h=\pm 2}\int d\Phi_k\left[a^h(k)\bar{\varepsilon}_{h\mu\nu}(k)e^{-ik\cdot r} + a^{h\dagger}(k)\varepsilon_{h\mu\nu}(k)e^{ik\cdot r}\right] \tag{A.5}$$

where we drop the unphysical modes for simplicity. The polarization tensors for the graviton are defined in terms of products of vector states as given by eq. (2.44). The measure factors and commutation conventions are,

$$d\Phi_k = \frac{d^D k}{(2\pi)^D}\,\theta(k^0)\hat{\delta}(k^2)\,, \quad \left[a^h(k), a^{h'\dagger}(k')\right] = (2E_k)\hat{\delta}^{D-1}(k-k')\delta^{hh'}\,. \tag{A.6}$$

and vanishing other commutators and we suppress un-physical modes.

Analogously, the massive vector and scalar fields are described by

$$\mathbb{V}^{\mu}(r) = \sum_{v=1}^{3}\int d\Phi_p\left[b^v(p)\bar{\varepsilon}^{\mu}_{v}(p)e^{-ip\cdot r} + b^{v\dagger}(p)\varepsilon^{\mu}_{v}(p)e^{ip\cdot r}\right], \tag{A.7}$$

$$\lesseqgtr(r) = \int d\Phi_p\left[b(p)e^{-ip\cdot r} + b^{\dagger}(p)e^{ip\cdot r}\right]. \tag{A.8}$$

To simplify the notation we will use the symbols b^s and $b^{s\dagger}$ to denote vector states and scalar states, with the index s labeling the different modes,

$$\{b^0(p),\, b^1(p),\, b^2(p)\,, b^3(p)\} = \{b(p),\, b^1(p),\, b^2(p),\, b^3(p)\}\,. \tag{A.9}$$

The mass m of the associated states is encoded by the square of the momentum argument $p^2 = m^2$. Phase space measure and creation/annihilation operators for matter the fields $\lesseqgtr$ and $\mathbb{V}^{\mu}$ are,

$$d\Phi_{p_i} = \frac{d^D p_i}{(2\pi)^D}\,\theta(p^0)\hat{\delta}(p_i^2 - m_i^2)\,, \quad \left[b^{s_1}(k), b^{s_2\dagger}(k')\right] = (2E_k)\hat{\delta}^{D-1}(k-k')\delta^{s_1 s_2}\,, \tag{A.10}$$

We use vector-boson polarisation states that are real and normalised,

$$\varepsilon_{v\mu}(p)\varepsilon^{\mu}_{v'}(p) = -\delta_{v'v}\,, \tag{A.11}$$

and

$$\bar{\varepsilon}_{v\mu}(p) = \varepsilon_{v\mu}(p)\,, \quad \bar{\varepsilon}_{v\mu}(p)\varepsilon_{v'\nu}(p)\delta^{vv'} = \frac{p_\mu p_\nu}{p^2} - \eta_{\mu\nu}\,. \tag{A.12}$$

To be explicit, we consider boosts of the configuration with momentum $p = (m, 0, 0, 0)$ and polarisation states pointing into e_x, e_y and e_z. Given that the boost are unique only up to little-group rotations, the basis of states is not unique either.

JHEP11(2024)109

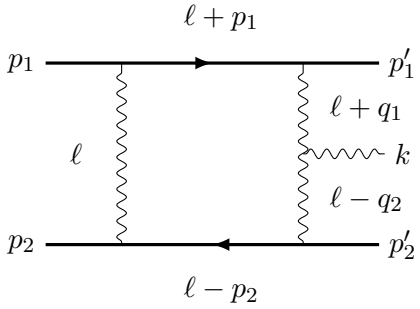

Figure 11. Topology A pentagon integral. The momenta $\{p_1, p_2\}$ are incoming, $\{p_1', p_2', k\}$ outgoing and ℓ flows clockwise in the diagram.

B Feynman integrals

In this section, we review the set of Feynman integrals required for the one-loop computation. We follow the ideas of ref. [60]. Representative Feynman diagrams of the five-point scattering process are shown in figure 4. We consider these diagrams in the classical limit. The pentagon integral family of topology A in figure 4 before the classical limit is given by

$$\mathcal{I}_A(\vec{\nu}) \equiv e^{\gamma_E \epsilon} \int \frac{d^D \ell}{i\pi^{D/2}} \frac{1}{\rho_1^{\nu_1} \rho_2^{\nu_2} \rho_3^{\nu_3} \rho_4^{\nu_4} \rho_5^{\nu_5}}, \tag{B.1}$$

with

$$\begin{aligned} &\rho_1 = \ell^2 + i\delta, && \rho_2 = (\ell + p_1)^2 - m_1^2 + i\delta, && \rho_3 = (\ell + q_1)^2 + i\delta, \\ &\rho_4 = (\ell - q_2)^2 + i\delta, && \rho_5 = (\ell - p_2)^2 - m_2^2 + i\delta. \end{aligned} \tag{B.2}$$

The vector $\vec{\nu} = (\nu_1, \nu_2, \nu_3, \nu_4, \nu_5)$ denotes the propagator powers. We are only interested in the classical limit of these integrals. Using the momentum parametrization in eq. (2.10) and taking the limit $\bar{m} \to \infty$ we obtain the following propagators,

$$\begin{aligned} &\rho_1 = \ell^2 + i\delta, && \rho_2 = 2(\ell \cdot u_1) + i\delta, && \rho_3 = (\ell + q_1)^2 + i\delta, \\ &\rho_4 = (\ell - q_2)^2 + i\delta, && \rho_5 = -2(\ell \cdot u_2) + i\delta. \end{aligned} \tag{B.3}$$

In the following, we denote the classical integral family simply by $\mathcal{I}_A(\vec{\nu})$, where we understand that all propagators are taken in their classical limit (see eq. (B.3)). For the classical integral family we construct a pure basis of 16 master integrals. First, we define the following 6 arguments of square roots,

$$r_1 = -q_1^2, \qquad r_2 = -q_2^2, \qquad r_3 = y^2 - 1, \tag{B.4}$$

$$r_4 = \omega_1^2 - q_2^2, \qquad r_5 = \omega_2^2 - q_1^2, \qquad \Delta_5 = G(u_1, u_2, q_1, q_2), \tag{B.5}$$

where we have defined the Gram determinant by

$$G(\{p_i\}) = \det(\{p_j \cdot p_k\}). \tag{B.6}$$

JHEP11(2024)109

Our choice of the 16 pure master integrals of $\mathcal{I}_A$ read,

$$\begin{aligned}
M_1^A &= \epsilon(1-2\epsilon)\,\mathcal{I}_A[1,0,1,0,0], & M_2^A &= \epsilon(1-2\epsilon)\,\mathcal{I}_A[1,0,0,1,0],\\
M_3^A &= \frac{\epsilon(1-2\epsilon)}{\omega_1}\,\mathcal{I}_A[0,1,0,1,0], & M_4^A &= \frac{\epsilon(1-2\epsilon)}{\omega_2}\,\mathcal{I}_A[0,0,1,0,1],\\
M_5^A &= \epsilon^2\sqrt{r_1}\,\mathcal{I}_A[1,1,1,0,0], & M_6^A &= \epsilon^2\sqrt{r_4}\,\mathcal{I}_A[1,1,0,1,0],\\
M_7^A &= \epsilon^2\sqrt{r_5}\,\mathcal{I}_A[1,0,1,0,1], & M_8^A &= \epsilon^2\sqrt{r_3}\,\mathcal{I}_A[0,1,1,0,1],\\
M_9^A &= \epsilon^2\sqrt{r_2}\,\mathcal{I}_A[1,0,0,1,1], & M_{10}^A &= \epsilon^2\sqrt{r_3}\,\mathcal{I}_A[0,1,0,1,1],\\
M_{11}^A &= \epsilon^2 q_1^2\,\omega_1\,\mathcal{I}_A[1,1,1,1,0], & M_{12}^A &= \epsilon^2\sqrt{r_3}\,q_1^2\,\mathcal{I}_A[1,1,1,0,1],\\
M_{13}^A &= \epsilon^2\sqrt{r_3}\,q_2^2\,\mathcal{I}_A[1,1,0,1,1], & M_{14}^A &= \epsilon^2 q_2^2\,\omega_2\,\mathcal{I}_A[1,0,1,1,1],\\
M_{15}^A &= \epsilon^2\omega_1\,\omega_2\,\mathcal{I}_A[0,1,1,1,1], & M_{16}^A &= \epsilon^2\sqrt{\Delta_5}\,\mathcal{I}_A[1,1,1,1,1][\mu_{11}].
\end{aligned} \tag{B.7}$$

Here $\mathcal{I}_A[1,1,1,1,1][\mu_{11}]$ denotes the insertion of the loop-momentum dependent numerator,

$$\mu_{11} = \frac{G(\ell,u_1,u_2,q_1,q_2)}{G(u_1,u_2,q_1,q_2)}, \tag{B.8}$$

for the pentagon integral that effectively shifts it to $d = 6-2\epsilon$ dimensions. The remaining classical integral families for the topologies shown in figure 4 can be conveniently obtained through,

$$\mathcal{I}_B \equiv \mathcal{I}_A|_{u_1\to -u_1}\,, \qquad \mathcal{I}_C \equiv \mathcal{I}_A|_{u_2\to -u_2}\,, \qquad \mathcal{I}_D \equiv \mathcal{I}_A|_{(u_1,u_2)\to -(u_1,u_2)}\,. \tag{B.9}$$

The same choice of basis (B.7) forms a pure basis also for $\mathcal{I}_B$, $\mathcal{I}_C$ and $\mathcal{I}_D$. These four integral families are sufficient to cover all occurring integrals in the classical limit. The reason for the reduced set of topologies is that in the limit $\bar{m}\to\infty$ propagators can become linearly dependent and can be reduced via partial fractioning. One example for such a case is the topology shown in figure 6, in which an external graviton emission from massive internal lines is present.

We now turn to the integrals required in the classical waveform observable, which combines classical integrals and classical limits of cut-integrals. Before the classical limit is taken we add the Cutkosky-cut contribution in the KMOC observable to all integrals (4.4). Among the integrals topologies A, B, C and D, only the family D has a non-vanishing cut in the $(p_1'+p_2')$-channel, which leads, according to ref. [60], to,

$$\mathcal{I}_D(\vec{\nu}) + \mathrm{Cut}_{1'2'}\,\mathcal{I}_D(\vec{\nu}) = \mathcal{I}_D(\vec{\nu}) - 2i\mathrm{Im}\left[\mathcal{I}_D(\vec{\nu})\right] = \left[\mathcal{I}_D(\vec{\nu})\right]^*. \tag{B.10}$$

After the classical limit is taken, we work with the complex conjugate integrals of family D. Given the scaling limit of integral coefficients the integrals appear in particular linear combinations. We define such linear combinations of master integrals and provide analytical results that are valid in the physical region of phase space given by eq. (2.12). We follow ref. [60] and define the linear combinations by,

$$\mathcal{I}^{\sigma_1,\sigma_2}(\vec{\nu}) \equiv \mathcal{I}_A(\vec{\nu}) + (-1)^{\nu_2}\sigma_1\,\mathcal{I}_B(\vec{\nu}) + \sigma_2(-1)^{\nu_5}\,\mathcal{I}_C(\vec{\nu}) + \sigma_1\sigma_2(-1)^{\nu_2+\nu_5}\left[\mathcal{I}_D(\vec{\nu})\right]^\star, \tag{B.11}$$

JHEP11(2024)109

where $\sigma_i = (-1)^{j_i}$ picks out the mass scaling $\bar{m}_1^{j_1}\bar{m}_2^{j_2}$. The pure basis is grouped analogously, as the algebraic prefactors are identical across all four topologies. Therefore, we refer to the linear combinations of eq. (B.11) applied to the master integrals of eq. (B.7) by,

$$M_n^{\sigma_1,\sigma_2}, \tag{B.12}$$

where n refers to the particular master integral. We compute the analytical expressions for the $M_n^{\pm\pm}$ integrals by numerical fitting. We compute high-precision numerical values for all master integrals M_n^X, with $X = A, B, C, D$, for all four integral families in the physical region using auxiliary mass flow method [135–137], as implemented in the AMFlow package [129]. We then combine the numerical values in the linear combinations of eq. (B.11) and obtain analytical expressions by fitting on weight-1 and 2 functions via the PLSQ algorithm provided by `PolyLogTools` [138]. Our results confirm the expressions of ref. [60].

For convenience, we now collect the results for the integral functions $M_n^{\pm\pm}$ in our conventions. All functions M_n^{--} vanish, while the functions,

$$M_n^{++} \neq 0, \tag{B.13}$$

drop out in the classical limit because of vanishing integral coefficients. The non-vanishing bubble integrals are,

$$M_3^{-+} = \epsilon\Big[-4i\pi\Big] + \epsilon^2\Big[4\pi^2 + 8i\pi\log(-2\omega_1)\Big] + \mathcal{O}(\epsilon^3), \tag{B.14}$$

$$M_4^{+-} = \epsilon\Big[-4i\pi\Big] + \epsilon^2\Big[4\pi^2 + 8i\pi\log(-2\omega_2)\Big] + \mathcal{O}(\epsilon^3). \tag{B.15}$$

The non-vanishing triangle integrals are,

$$M_5^{-+} = \epsilon^2\Big[-2\pi^2\Big] + \mathcal{O}(\epsilon^3), \tag{B.16}$$

$$M_6^{-+} = \epsilon^2\left[-2\pi^2 - 2i\pi\log\left(\frac{\sqrt{r_4}-\omega_1}{\sqrt{r_4}+\omega_1}\right)\right] + \mathcal{O}(\epsilon^3), \tag{B.17}$$

$$M_7^{+-} = \epsilon^2\left[-2\pi^2 - 2i\pi\log\left(\frac{\sqrt{r_5}-\omega_2}{\sqrt{r_5}+\omega_2}\right)\right] + \mathcal{O}(\epsilon^3), \tag{B.18}$$

$$M_8^{-+} = \epsilon\Big[-i\pi\Big] + \epsilon^2\left[\pi^2 - i\pi\log\left(\frac{y^2-1}{\omega_2^2}\right)\right] + \mathcal{O}(\epsilon^3), \tag{B.19}$$

$$M_8^{+-} = \epsilon\Big[-i\pi\Big] + \epsilon^2\left[\pi^2 + 2i\pi\log(y+\sqrt{r_3}) - i\pi\log\left(\frac{y^2-1}{\omega_2^2}\right)\right] + \mathcal{O}(\epsilon^3), \tag{B.20}$$

$$M_9^{+-} = \epsilon^2\Big[-2\pi^2\Big] + \mathcal{O}(\epsilon^3), \tag{B.21}$$

$$M_{10}^{-+} = \epsilon\Big[-i\pi\Big] + \epsilon^2\left[\pi^2 + 2i\pi\log(y+\sqrt{r_3}) - i\pi\log\left(\frac{y^2-1}{\omega_1^2}\right)\right] + \mathcal{O}(\epsilon^3), \tag{B.22}$$

$$M_{10}^{+-} = \epsilon\Big[-i\pi\Big] + \epsilon^2\left[\pi^2 - i\pi\log\left(\frac{y^2-1}{\omega_1^2}\right)\right] + \mathcal{O}(\epsilon^3). \tag{B.23}$$

JHEP11(2024)109

The non-vanishing box integrals are,

$$M_{11}^{-+} = \epsilon\Big[-i\pi\Big] + \epsilon^2\left[\pi^2 - i\pi\log\left(\frac{q_2^4}{4\omega_1^2 q_1^4}\right)\right] + \mathcal{O}(\epsilon^3), \tag{B.24}$$

$$M_{12}^{-+} = \epsilon\Big[i\pi\Big] + \epsilon^2\left[\pi^2 - i\pi\log\left(\frac{q_1^4(y^2-1)}{\omega_2^2}\right)\right] + \mathcal{O}(\epsilon^3), \tag{B.25}$$

$$M_{12}^{+-} = \epsilon\Big[i\pi\Big] + \epsilon^2\left[\pi^2 + 2i\pi\log(y+\sqrt{r_3}) - i\pi\log\left(\frac{q_1^4(y^2-1)}{\omega_2^2}\right)\right] + \mathcal{O}(\epsilon^3), \tag{B.26}$$

$$M_{13}^{-+} = \epsilon\Big[i\pi\Big] + \epsilon^2\left[\pi^2 + 2i\pi\log(y+\sqrt{r_3}) - i\pi\log\left(\frac{q_2^4(y^2-1)}{\omega_1^2}\right)\right] + \mathcal{O}(\epsilon^3), \tag{B.27}$$

$$M_{13}^{+-} = \epsilon\Big[i\pi\Big] + \epsilon^2\left[\pi^2 - i\pi\log\left(\frac{q_2^4(y^2-1)}{\omega_1^2}\right)\right] + \mathcal{O}(\epsilon^3), \tag{B.28}$$

$$M_{14}^{+-} = \epsilon\Big[-i\pi\Big] + \epsilon^2\left[\pi^2 - i\pi\log\left(\frac{q_1^4}{4\omega_2^2 q_2^4}\right)\right] + \mathcal{O}(\epsilon^3), \tag{B.29}$$

$$M_{15}^{-+} = \epsilon\Big[\frac{i\pi}{2}\Big] + \epsilon^2\left[-\frac{\pi^2}{2} + i\pi\log(y+\sqrt{r_3}) - \frac{i\pi}{2}\log\left(4\omega_2^2\right)\right] + \mathcal{O}(\epsilon^3), \tag{B.30}$$

$$M_{15}^{+-} = \epsilon\Big[\frac{i\pi}{2}\Big] + \epsilon^2\left[-\frac{\pi^2}{2} + i\pi\log(y+\sqrt{r_3}) - \frac{i\pi}{2}\log\left(4\omega_1^2\right)\right] + \mathcal{O}(\epsilon^3). \tag{B.31}$$

The pentagon integrals contribute only to higher orders in ϵ,

$$M_{16}^{\pm\mp} = \mathcal{O}(\epsilon^3)\,, \tag{B.32}$$

and are not required for the one-loop results.

To obtain the necessary integrals in the physical normalization, a factor of,

$$\tilde{c}_N = \frac{i}{(4\pi)^2}\left(4\pi\mu^2 e^{-\gamma_E}\right)^{\epsilon}, \tag{B.33}$$

needs to be included. In the supplementary material we group another fartor of π with this normalisation using $c_N = -\pi\tilde{c}_N$.

The final result for the spectral waveform is written in terms of linearly independent special functions f_i that we collect here for completeness. The functions,

$$f_1 = i\pi, \qquad f_2 = \frac{i\pi}{\sqrt{y^2-1}}, \tag{B.34}$$

$$f_3 = \frac{2\log\left(\frac{\sqrt{\omega_1^2-q_2^2}-\omega_1}{\sqrt{-q_2^2}}\right) - i\pi}{\sqrt{\omega_1^2-q_2^2}}, \qquad f_4 = \frac{-i\pi}{\sqrt{-q_1^2}}, \tag{B.35}$$

$$f_5 = \log\left(\frac{\omega_2^2}{\omega_1^2}\right), \qquad f_6 = \log(4)\,, \tag{B.36}$$

$$f_7 = \log\left(\frac{q_1^2}{q_2^2}\right), \qquad f_8 = \frac{\log\left(y+\sqrt{y^2-1}\right)}{\sqrt{y^2-1}}, \tag{B.37}$$

$$f_9 = \gamma_E - \log(\pi), \qquad f_{10} = 1, \tag{B.38}$$

JHEP11(2024)109

$$f_{11} = \frac{2\log\left(\frac{\sqrt{\omega_2^2-q_1^2}-\omega_2}{\sqrt{-q_1^2}}\right) - i\pi}{\sqrt{\omega_2^2-q_1^2}}, \qquad f_{12} = \frac{-i\pi}{\sqrt{-q_2^2}}, \tag{B.39}$$

$$f_{13} = \frac{1}{\sqrt{y^2-1}}, \qquad f_{14} = \frac{\log\left((y^2-1)\frac{\omega_2}{\omega_1}\right)}{\sqrt{y^2-1}}, \tag{B.40}$$

$$f_{15} = \frac{\log\left((y^2-1)\frac{\omega_1}{\omega_2}\right)}{\sqrt{y^2-1}}, \qquad f_{16} = \frac{\log\left(\frac{-q_1^2}{\omega_1\omega_2}\right)}{\sqrt{y^2-1}}, \tag{B.41}$$

$$f_{17} = \frac{\log\left(\frac{-q_2^2}{\omega_1\omega_2}\right)}{\sqrt{y^2-1}}, \qquad f_{18} = \log\left(y+\sqrt{y^2-1}\right), \tag{B.42}$$

span the basis of $\mathcal{M}^{\text{finite}}$, while the remaining regulator dependent functions are necessary to express the $\mathcal{M}^{\text{UV}}$, $\mathcal{M}^{\text{IR}}$ and $\mathcal{M}^{\text{tail}}$ parts of the waveform:

$$f_{19} = \log\left(\frac{\omega_1\omega_2}{\mu_{\text{IR}}^2}\right), \qquad f_{20/21} = \frac{\log\left(\frac{\omega_1\omega_2}{\mu_{\text{IR/UV}}^2}\right)}{\sqrt{y^2-1}}, \tag{B.43}$$

$$f_{22} = \log\left(\frac{\mu^2}{\mu_{\text{IR}}^2}\right), \qquad f_{23/24} = \frac{\log\left(\frac{\mu^2}{\mu_{\text{IR/UV}}^2}\right)}{\sqrt{y^2-1}}. \tag{B.44}$$

C IR divergence of waveform observable

Scattering amplitudes of matter coupled to gravity exhibit universal infrared singularities [103]. Here we collect the known results, following ref. [57]. The infrared divergence of a n-point one-loop amplitude is proportional to tree amplitudes,

$$M^{1-\text{loop},\vec{s}}(p_i) = \frac{1}{\epsilon} W_S(p_i)\, M^{\text{tree},\vec{s}}(p_i)\,, \tag{C.1}$$

for n particles with momentum $p_i^2 = m_i^2$ and mass m_i, which may be vanishing. Total momentum is conserved $p_1 + p_2 = p_1' + p_2' + k$. For the main text we consider the five-point processes (2.8) and (2.9).

The soft factor W_S arises from soft graviton exchanges between pairs of distinct scattering particles. The contribution from particle i and $j \neq i$ is given by,

$$\beta_{ij} = \sqrt{1 - \frac{m_i^2 m_j^2}{(p_i\cdot p_j)^2}}\,, \tag{C.2}$$

$$c_{ij} = \begin{cases} m_i = 0 \text{ or } m_j = 0\,, & \frac{G}{2\pi}\, 4(p_i\cdot p_j)\,, \\ \text{else}\,, & \frac{G}{2\pi}\,\frac{(p_i\cdot p_j)(1+\beta_{ij}^2)}{\beta_{ij}}\,, \end{cases} \tag{C.3}$$

$$f_{ij} = \begin{cases} m_i = 0 \text{ or } m_j = 0\,, & \log\left|\frac{2(p_i\cdot p_j)}{\mu_{\text{IR}}^2}\right| - \pi i\Theta[(p_i\cdot p_j)]\,, \\ \text{else}\,, & \log\left[\frac{1+\beta_{ij}}{1-\beta_{ij}}\right] - 2\pi i\Theta[(p_i\cdot p_j)]. \end{cases} \tag{C.4}$$

For emission and absorption by the same external line, the imaginary parts are absent and one has to rearrange the equations.

JHEP11(2024)109

For the imaginary contribution one considers all pairs of initial-state and all pairs of final-state particles,

$$i\,\mathrm{Im}\Big[W_S\Big] = \frac{1}{4}\sum_{\substack{i,j=1\\ i\neq j}}^{n} c_{ij}\,f_{ij} = -\frac{i\pi}{2}(2c_{12}+2c_{1'2'}+c_{1'k}+c_{2'k})\,. \tag{C.5}$$

For the waveform observable we need to add the cut in the $(p_1'+p_2')$-channel from the 1-loop amplitude. This cut is associated to the function $f_{1'2'}$, which is the triangle function with the external legs p_1' and p_2'. Before taking the classical limit the cut can be obtained as the branch cut of $f_{1'2'}$ in the analytic continuation in $s_{1'2'}$, which evaluates to $-2ic_{1'2'}\mathrm{Im}(f_{1'2'})$. Adding this cut then yields the imaginary part of the waveform soft factor,

$$i\,\mathrm{Im}\Big[\mathcal{W}_S\Big] = i\,\mathrm{Im}\Big[W_S\Big] + \mathrm{Cut}_{1'2'}(W_S) = -\frac{i\pi}{2}(2c_{12}-2c_{1'2'}+c_{1'k}+c_{2'k})\,, \tag{C.6}$$

effectively, flipping the sign of the $c_{1'2'}$ contribution. Plugging in the kinematic expressions and taking the classical limit we obtain,

$$\mathcal{W}_S = W_S + \mathrm{Cut}_{1'2'}(W_S) = iG(\bar{m}_1\omega_1+\bar{m}_2\omega_2)\left[1+\frac{y(2y^2-3)}{2(y^2-1)^{3/2}}\right]. \tag{C.7}$$

We observe that the hyper-classical terms cancel and that the classical contribution of the real part of the IR divergence vanishes [57] as well.

D Momentum parameterization

As discussed in section 4.5, we employ functional reconstruction techniques to obtain analytical expressions for the classical amplitudes. The necessary numerical values for this procedure are generated using Caravel.

For convenience and efficiency, we work in finite-field ($\mathbb{F}_p$) arithmetic, therefore we require a $\mathbb{F}_p$ parameterization of the external momenta and polarization states. We obtain the parameterization from rotations and boosts of a generic momentum configuration and use rational representations of $\sin$, $\cos$, $\sinh$ and $\cosh$ functions,

$$\sin_r(x) = \frac{2x}{x^2+1}, \qquad \cos_r(x) = \frac{x^2-1}{x^2+1}, \tag{D.1}$$

$$\sinh_r(x) = \frac{2x}{x^2-1}, \qquad \cosh_r(x) = \frac{x^2+1}{x^2-1}, \tag{D.2}$$

which fulfill,

$$\sin_r^2(x)+\cos_r^2(x) = 1, \qquad \cosh_r^2(x)-\sinh_r^2(x) = 1. \tag{D.3}$$

In order to avoid complex-valued helicity states we work in an alternating metric signature,

$$\eta = \mathrm{diag}\{1,-1,1,-1\}. \tag{D.4}$$

In this signature one can construct Majorana-Weyl spinors, i.e. real-valued helicity spinors. This does not imply any loss of generality, if we extract rational expressions in momentum

JHEP11(2024)109

invariants $s_{ij} = (p_1 + p_j)^2$. However, we will need to pay attention to the metric convention in boosts and the phase-space parameterization.

We can construct a momentum parameterization for p_1, p_2, p_1', p_2' and k in the all outgoing convention, as this is the natural parameterization used in Caravel. It is enough to obtain momenta for u_1, u_2, q_1 and q_2 to obtain a full set of external momenta by,

$$\begin{aligned} p_1 &= \bar{m}_1 u_1 + \frac{q_1}{2}, \qquad & p_1' &= -\bar{m}_1 u_1 + \frac{q_1}{2}, \\ p_2 &= \bar{m}_2 u_2 + \frac{q_2}{2}, \qquad & p_2' &= -\bar{m}_2 u_2 + \frac{q_2}{2}, \qquad & k &= -(q_1 + q_2). \end{aligned} \tag{D.5}$$

We define the velocities u_1 and u_2 by,

$$u_1^\mu = \begin{pmatrix} 1 \\ 0 \\ 0 \\ 0 \end{pmatrix}, \quad u_2^\mu = \begin{pmatrix} \cosh_r(x) \\ \sinh_r(x) \\ 0 \\ 0 \end{pmatrix}, \tag{D.6}$$

while the momentum transfer vectors q_i read,

$$q_1^\mu = r_1 \begin{pmatrix} 0 \\ \sinh_r(t_1) \\ \cosh_r(t_1) \\ 0 \end{pmatrix}, \quad q_2^\mu = r_2 \begin{pmatrix} \sinh_r(t_2)\sinh_r(x) \\ \sinh_r(t_2)\cosh_r(x) \\ \cosh_r(t_2)\cosh_r(t_3) \\ \cosh_r(t_2)\sinh_r(t_3) \end{pmatrix}. \tag{D.7}$$

The relations between the physical invariants and these parameterizations are given by,

$$\begin{aligned} y &= u_1 \cdot u_2 = \cosh_r(x), \qquad & q_1^2 &= r_1^2, \qquad & q_2^2 &= r_2^2, \\ \omega_1 &= k \cdot u_1 = -r_2 \sinh_r(t_2)\sinh_r(x), \qquad & \omega_2 &= k \cdot u_2 = r_1 \sinh_r(t_1)\sinh_r(x). \end{aligned} \tag{D.8}$$

At this point, the momenta are functions of the above auxiliary variables,

$$\{r_1, r_2, t_1, t_2, t_3, x\}, \tag{D.9}$$

and in the mass parameters $\bar{m}_1$ and $\bar{m}_2$. All of them, except for t_3, are related to the kinematical invariants. The variable t_3 is defined through the on-shellness of the graviton momenta, i.e. $k^2 = 0$, and is given by

$$t_3 = \sqrt{\frac{r_1^2 + r_2^2 - 2r_1 r_2 \left[\cosh_r(t_1)\cosh_r(t_2) + \cosh_r(x)\sinh_r(t_1)\sinh_r(t_2)\right]}{r_1^2 + r_2^2 + 2r_1 r_2 \left[\cosh_r(t_1)\cosh_r(t_2) - \cosh_r(x)\sinh_r(t_1)\sinh_r(t_2)\right]}}. \tag{D.10}$$

With this we have an algebraic parameterization of phase space because of the square root in the function t_3. However, the dependence on the kinematic invariants is rational. The momenta are then generated as follows,

1. Generate random values for $\{r_1, r_2, t_1, t_2, x\} \in \mathbb{F}_p$, such that t_3 has a solution in $\mathbb{F}_p$.

2. Generate random values for $\bar{m}_1$ and $\bar{m}_2$ such that

$$\sqrt{\bar{m}_i + \frac{q_i^2}{4}} \in \mathbb{F}_p. \tag{D.11}$$

JHEP11(2024)109

3. Construct the momenta according to eq. (D.5).

All square roots are taken in $\mathbb{F}_p$, i.e. for $r = \sqrt{s}$ one searches a number r in $\mathbb{F}_p$ with,

$$r^2 \bmod p = s, \tag{D.12}$$

This number cannot always be found, as the field is not algebraically complete. However, squares are frequent (approx. 50% chance) in finite fields and random sampling of input parameters until all square roots can be taken, is sufficiently efficient.

Data Availability Statement. This article has no associated data or the data will not be deposited.

Code Availability Statement. This article has code included as electronic supplementary material.

References

[1] LIGO Scientific and Virgo collaborations, *GW151226: Observation of Gravitational Waves from a 22-Solar-Mass Binary Black Hole Coalescence*, *Phys. Rev. Lett.* **116** (2016) 241103 [arXiv:1606.04855] [INSPIRE].

[2] LIGO Scientific and Virgo collaborations, *Binary Black Hole Mergers in the first Advanced LIGO Observing Run*, *Phys. Rev. X* **6** (2016) 041015 [*Erratum ibid.* **8** (2018) 039903] [arXiv:1606.04856] [INSPIRE].

[3] KAGRA et al. collaborations, *GWTC-3: Compact Binary Coalescences Observed by LIGO and Virgo during the Second Part of the Third Observing Run*, *Phys. Rev. X* **13** (2023) 041039 [arXiv:2111.03606] [INSPIRE].

[4] D. Reitze et al., *Cosmic Explorer: the U.S. Contribution to Gravitational-Wave Astronomy beyond LIGO*, *Bull. Am. Astron. Soc.* **51** (2019) 035 [arXiv:1907.04833] [INSPIRE].

[5] M. Punturo et al., *The Einstein Telescope: a third-generation gravitational wave observatory*, *Class. Quant. Grav.* **27** (2010) 194002 [INSPIRE].

[6] LISA collaboration, *Laser Interferometer Space Antenna*, arXiv:1702.00786 [INSPIRE].

[7] A. Buonanno and T. Damour, *Effective one-body approach to general relativistic two-body dynamics*, *Phys. Rev. D* **59** (1999) 084006 [gr-qc/9811091] [INSPIRE].

[8] A. Buonanno and T. Damour, *Transition from inspiral to plunge in binary black hole coalescences*, *Phys. Rev. D* **62** (2000) 064015 [gr-qc/0001013] [INSPIRE].

[9] L. Blanchet, *Post-Newtonian Theory for Gravitational Waves*, *Living Rev. Rel.* **17** (2014) 2 [arXiv:1310.1528] [INSPIRE].

[10] G. Schäfer and P. Jaranowski, *Hamiltonian formulation of general relativity and post-Newtonian dynamics of compact binaries*, *Living Rev. Rel.* **21** (2018) 7 [arXiv:1805.07240] [INSPIRE].

JHEP11(2024)109

[11] Y. Mino, M. Sasaki and T. Tanaka, *Gravitational radiation reaction to a particle motion*, *Phys. Rev. D* **55** (1997) 3457 [gr-qc/9606018] [INSPIRE].

[12] T.C. Quinn and R.M. Wald, *An axiomatic approach to electromagnetic and gravitational radiation reaction of particles in curved space-time*, *Phys. Rev. D* **56** (1997) 3381 [gr-qc/9610053] [INSPIRE].

[13] W.D. Goldberger and I.Z. Rothstein, *An effective field theory of gravity for extended objects*, *Phys. Rev. D* **73** (2006) 104029 [hep-th/0409156] [INSPIRE].

[14] W.D. Goldberger and I.Z. Rothstein, *Towers of Gravitational Theories*, *Gen. Rel. Grav.* **38** (2006) 1537 [hep-th/0605238] [INSPIRE].

[15] W.D. Goldberger and A. Ross, *Gravitational radiative corrections from effective field theory*, *Phys. Rev. D* **81** (2010) 124015 [arXiv:0912.4254] [INSPIRE].

[16] R.A. Porto, A. Ross and I.Z. Rothstein, *Spin induced multipole moments for the gravitational wave amplitude from binary inspirals to 2.5 Post-Newtonian order*, *JCAP* **09** (2012) 028 [arXiv:1203.2962] [INSPIRE].

[17] L. Blanchet and B.S. Sathyaprakash, *Detecting the tail effect in gravitational wave experiments*, *Phys. Rev. Lett.* **74** (1995) 1067 [INSPIRE].

[18] A. Einstein and L. Infeld, *The gravitational equations and the problem of motion. 2*, *Annals Math.* **41** (1940) 455 [INSPIRE].

[19] B. Bertotti, *On gravitational motion*, *Nuovo Cim.* **4** (1956) 898 [INSPIRE].

[20] R.P. Kerr, *The Lorentz-covariant approximation method in general relativity I*, *Nuovo Cim.* **13** (1959) 469 [INSPIRE].

[21] B. Bertotti and J. Plebanski, *Theory of gravitational perturbations in the fast motion approximation*, *Annals Phys.* **11** (1960) 169 [INSPIRE].

[22] M. Portilla, *Momentum and angular momentum of two gravitating particles*, *J. Phys. A* **12** (1979) 1075 [INSPIRE].

[23] K. Westpfahl and M. Goller, *Gravitational scattering of two relativistic particles in postlinear approximation*, *Lett. Nuovo Cim.* **26** (1979) 573 [INSPIRE].

[24] M. Portilla, *Scattering of two gravitating particles: classical approach*, *J. Phys. A* **13** (1980) 3677 [INSPIRE].

[25] L.L. Bel et al., *Poincaré-invariant gravitational field and equations of motion of two pointlike objects: the postlinear approximation of general relativity*, *Gen. Rel. Grav.* **13** (1981) 963 [INSPIRE].

[26] K. Westpfahl, *High-Speed Scattering of Charged and Uncharged Particles in General Relativity*, *Fortsch. Phys.* **33** (1985) 417 [INSPIRE].

[27] T. Damour, *Gravitational scattering, post-Minkowskian approximation and Effective One-Body theory*, *Phys. Rev. D* **94** (2016) 104015 [arXiv:1609.00354] [INSPIRE].

[28] T. Ledvinka, G. Schaefer and J. Bicak, *Relativistic Closed-Form Hamiltonian for Many-Body Gravitating Systems in the Post-Minkowskian Approximation*, *Phys. Rev. Lett.* **100** (2008) 251101 [arXiv:0807.0214] [INSPIRE].

[29] Z. Bern et al., *Scattering Amplitudes and the Conservative Hamiltonian for Binary Systems at Third Post-Minkowskian Order*, *Phys. Rev. Lett.* **122** (2019) 201603 [arXiv:1901.04424] [INSPIRE].

JHEP11(2024)109

[30] Z. Bern et al., *Scattering Amplitudes and Conservative Binary Dynamics at $\mathcal{O}(G^4)$*, *Phys. Rev. Lett.* **126** (2021) 171601 [arXiv:2101.07254] [INSPIRE].

[31] Z. Bern et al., *Scattering Amplitudes, the Tail Effect, and Conservative Binary Dynamics at O(G4)*, *Phys. Rev. Lett.* **128** (2022) 161103 [arXiv:2112.10750] [INSPIRE].

[32] C. Dlapa, G. Kälin, Z. Liu and R.A. Porto, *Dynamics of binary systems to fourth Post-Minkowskian order from the effective field theory approach*, *Phys. Lett. B* **831** (2022) 137203 [arXiv:2106.08276] [INSPIRE].

[33] G. Kälin, J. Neef and R.A. Porto, *Radiation-reaction in the Effective Field Theory approach to Post-Minkowskian dynamics*, *JHEP* **01** (2023) 140 [arXiv:2207.00580] [INSPIRE].

[34] C. Dlapa et al., *Radiation Reaction and Gravitational Waves at Fourth Post-Minkowskian Order*, *Phys. Rev. Lett.* **130** (2023) 101401 [arXiv:2210.05541] [INSPIRE].

[35] M. Khalil, A. Buonanno, J. Steinhoff and J. Vines, *Energetics and scattering of gravitational two-body systems at fourth post-Minkowskian order*, *Phys. Rev. D* **106** (2022) 024042 [arXiv:2204.05047] [INSPIRE].

[36] P. Rettegno et al., *Strong-field scattering of two spinning black holes: numerical relativity versus post-Minkowskian gravity*, *Phys. Rev. D* **108** (2023) 124016 [arXiv:2307.06999] [INSPIRE].

[37] P.H. Damgaard, K. Haddad and A. Helset, *Heavy Black Hole Effective Theory*, *JHEP* **11** (2019) 070 [arXiv:1908.10308] [INSPIRE].

[38] R. Aoude, K. Haddad and A. Helset, *On-shell heavy particle effective theories*, *JHEP* **05** (2020) 051 [arXiv:2001.09164] [INSPIRE].

[39] K. Haddad and A. Helset, *The double copy for heavy particles*, *Phys. Rev. Lett.* **125** (2020) 181603 [arXiv:2005.13897] [INSPIRE].

[40] A. Brandhuber, G. Chen, G. Travaglini and C. Wen, *A new gauge-invariant double copy for heavy-mass effective theory*, *JHEP* **07** (2021) 047 [arXiv:2104.11206] [INSPIRE].

[41] G. Kälin, Z. Liu and R.A. Porto, *Conservative Dynamics of Binary Systems to Third Post-Minkowskian Order from the Effective Field Theory Approach*, *Phys. Rev. Lett.* **125** (2020) 261103 [arXiv:2007.04977] [INSPIRE].

[42] Z. Liu, R.A. Porto and Z. Yang, *Spin Effects in the Effective Field Theory Approach to Post-Minkowskian Conservative Dynamics*, *JHEP* **06** (2021) 012 [arXiv:2102.10059] [INSPIRE].

[43] G. Kälin and R.A. Porto, *Post-Minkowskian Effective Field Theory for Conservative Binary Dynamics*, *JHEP* **11** (2020) 106 [arXiv:2006.01184] [INSPIRE].

[44] P. Di Vecchia, C. Heissenberg, R. Russo and G. Veneziano, *The eikonal approach to gravitational scattering and radiation at $\mathcal{O}(G^3)$*, *JHEP* **07** (2021) 169 [arXiv:2104.03256] [INSPIRE].

[45] P. Di Vecchia, C. Heissenberg, R. Russo and G. Veneziano, *The eikonal operator at arbitrary velocities I: the soft-radiation limit*, *JHEP* **07** (2022) 039 [arXiv:2204.02378] [INSPIRE].

[46] P. Di Vecchia, C. Heissenberg, R. Russo and G. Veneziano, *Classical gravitational observables from the Eikonal operator*, *Phys. Lett. B* **843** (2023) 138049 [arXiv:2210.12118] [INSPIRE].

[47] A. Luna, N. Moynihan, D. O'Connell and A. Ross, *Observables from the spinning eikonal*, *JHEP* **08** (2024) 045 [arXiv:2312.09960] [INSPIRE].

[48] D.A. Kosower, B. Maybee and D. O'Connell, *Amplitudes, Observables, and Classical Scattering*, *JHEP* **02** (2019) 137 [arXiv:1811.10950] [INSPIRE].

JHEP11(2024)109

[49] B. Maybee, D. O'Connell and J. Vines, *Observables and amplitudes for spinning particles and black holes*, *JHEP* **12** (2019) 156 [arXiv:1906.09260] [INSPIRE].

[50] A. Cristofoli, R. Gonzo, D.A. Kosower and D. O'Connell, *Waveforms from amplitudes*, *Phys. Rev. D* **106** (2022) 056007 [arXiv:2107.10193] [INSPIRE].

[51] G.U. Jakobsen, G. Mogull, J. Plefka and J. Steinhoff, *Classical Gravitational Bremsstrahlung from a Worldline Quantum Field Theory*, *Phys. Rev. Lett.* **126** (2021) 201103 [arXiv:2101.12688] [INSPIRE].

[52] G.U. Jakobsen, G. Mogull, J. Plefka and J. Steinhoff, *Gravitational Bremsstrahlung and Hidden Supersymmetry of Spinning Bodies*, *Phys. Rev. Lett.* **128** (2022) 011101 [arXiv:2106.10256] [INSPIRE].

[53] S. Mougiakakos, M.M. Riva and F. Vernizzi, *Gravitational Bremsstrahlung in the post-Minkowskian effective field theory*, *Phys. Rev. D* **104** (2021) 024041 [arXiv:2102.08339] [INSPIRE].

[54] S.J. Kovacs and K.S. Thorne, *The Generation of Gravitational Waves. 3. Derivation of Bremsstrahlung Formulas*, *Astrophys. J.* **217** (1977) 252 [INSPIRE].

[55] S.J. Kovacs and K.S. Thorne, *The Generation of Gravitational Waves. 4. Bremsstrahlung*, *Astrophys. J.* **224** (1978) 62 [INSPIRE].

[56] A. Herderschee, R. Roiban and F. Teng, *The sub-leading scattering waveform from amplitudes*, *JHEP* **06** (2023) 004 [arXiv:2303.06112] [INSPIRE].

[57] A. Brandhuber et al., *One-loop gravitational bremsstrahlung and waveforms from a heavy-mass effective field theory*, *JHEP* **06** (2023) 048 [arXiv:2303.06111] [INSPIRE].

[58] A. Georgoudis, C. Heissenberg and I. Vazquez-Holm, *Inelastic exponentiation and classical gravitational scattering at one loop*, *JHEP* **06** (2023) 126 [arXiv:2303.07006] [INSPIRE].

[59] A. Elkhidir, D. O'Connell, M. Sergola and I.A. Vazquez-Holm, *Radiation and reaction at one loop*, *JHEP* **07** (2024) 272 [arXiv:2303.06211] [INSPIRE].

[60] S. Caron-Huot, M. Giroux, H.S. Hannesdottir and S. Mizera, *What can be measured asymptotically?*, *JHEP* **01** (2024) 139 [arXiv:2308.02125] [INSPIRE].

[61] D. Bini, T. Damour and A. Geralico, *Comparing one-loop gravitational bremsstrahlung amplitudes to the multipolar-post-Minkowskian waveform*, *Phys. Rev. D* **108** (2023) 124052 [arXiv:2309.14925] [INSPIRE].

[62] A. Georgoudis, C. Heissenberg and R. Russo, *An eikonal-inspired approach to the gravitational scattering waveform*, *JHEP* **03** (2024) 089 [arXiv:2312.07452] [INSPIRE].

[63] D. Bini and T. Damour, *Gravitational spin-orbit coupling in binary systems, post-Minkowskian approximation and effective one-body theory*, *Phys. Rev. D* **96** (2017) 104038 [arXiv:1709.00590] [INSPIRE].

[64] J. Vines, *Scattering of two spinning black holes in post-Minkowskian gravity, to all orders in spin, and effective-one-body mappings*, *Class. Quant. Grav.* **35** (2018) 084002 [arXiv:1709.06016] [INSPIRE].

[65] D. Bini and T. Damour, *Gravitational spin-orbit coupling in binary systems at the second post-Minkowskian approximation*, *Phys. Rev. D* **98** (2018) 044036 [arXiv:1805.10809] [INSPIRE].

[66] Z. Bern et al., *Spinning black hole binary dynamics, scattering amplitudes, and effective field theory*, *Phys. Rev. D* **104** (2021) 065014 [arXiv:2005.03071] [INSPIRE].

JHEP11(2024)109

[67] Y.F. Bautista, A. Guevara, C. Kavanagh and J. Vines, *Scattering in black hole backgrounds and higher-spin amplitudes. Part II*, *JHEP* **05** (2023) 211 [arXiv:2212.07965] [INSPIRE].

[68] Y.F. Bautista et al., *Black hole perturbation theory meets CFT2: Kerr-Compton amplitudes from Nekrasov-Shatashvili functions*, *Phys. Rev. D* **109** (2024) 084071 [arXiv:2312.05965] [INSPIRE].

[69] G.U. Jakobsen et al., *Conservative Scattering of Spinning Black Holes at Fourth Post-Minkowskian Order*, *Phys. Rev. Lett.* **131** (2023) 151401 [arXiv:2306.01714] [INSPIRE].

[70] G.U. Jakobsen, G. Mogull, J. Plefka and B. Sauer, *Dissipative Scattering of Spinning Black Holes at Fourth Post-Minkowskian Order*, *Phys. Rev. Lett.* **131** (2023) 241402 [arXiv:2308.11514] [INSPIRE].

[71] F. Febres Cordero et al., *Conservative Binary Dynamics with a Spinning Black Hole at O(G3) from Scattering Amplitudes*, *Phys. Rev. Lett.* **130** (2023) 021601 [arXiv:2205.07357] [INSPIRE].

[72] Z. Bern et al., *Binary Dynamics through the Fifth Power of Spin at O(G2)*, *Phys. Rev. Lett.* **130** (2023) 201402 [arXiv:2203.06202] [INSPIRE].

[73] R. Aoude, K. Haddad and A. Helset, *Classical Gravitational Spinning-Spinless Scattering at O(G2S∞)*, *Phys. Rev. Lett.* **129** (2022) 141102 [arXiv:2205.02809] [INSPIRE].

[74] R. Aoude, K. Haddad and A. Helset, *Classical gravitational scattering amplitude at O(G2S1∞S2∞)*, *Phys. Rev. D* **108** (2023) 024050 [arXiv:2304.13740] [INSPIRE].

[75] M. Chiodaroli, H. Johansson and P. Pichini, *Compton black-hole scattering for $s \leq 5/2$*, *JHEP* **02** (2022) 156 [arXiv:2107.14779] [INSPIRE].

[76] L. Cangemi and P. Pichini, *Classical limit of higher-spin string amplitudes*, *JHEP* **06** (2023) 167 [arXiv:2207.03947] [INSPIRE].

[77] L. Cangemi et al., *Kerr Black Holes From Massive Higher-Spin Gauge Symmetry*, *Phys. Rev. Lett.* **131** (2023) 221401 [arXiv:2212.06120] [INSPIRE].

[78] A. Ochirov and E. Skvortsov, *Chiral Approach to Massive Higher Spins*, *Phys. Rev. Lett.* **129** (2022) 241601 [arXiv:2207.14597] [INSPIRE].

[79] L. Cangemi et al., *From higher-spin gauge interactions to Compton amplitudes for root-Kerr*, *JHEP* **09** (2024) 196 [arXiv:2311.14668] [INSPIRE].

[80] F. Alessio, *Kerr binary dynamics from minimal coupling and double copy*, *JHEP* **04** (2024) 058 [arXiv:2303.12784] [INSPIRE].

[81] G. Menezes and M. Sergola, *NLO deflections for spinning particles and Kerr black holes*, *JHEP* **10** (2022) 105 [arXiv:2205.11701] [INSPIRE].

[82] V. Vaidya, *Gravitational spin Hamiltonians from the S matrix*, *Phys. Rev. D* **91** (2015) 024017 [arXiv:1410.5348] [INSPIRE].

[83] S. De Angelis, P.P. Novichkov and R. Gonzo, *Spinning waveforms from the Kosower-Maybee-O'Connell formalism at leading order*, *Phys. Rev. D* **110** (2024) L041502 [arXiv:2309.17429] [INSPIRE].

[84] A. Brandhuber et al., *Resummed spinning waveforms from five-point amplitudes*, *JHEP* **02** (2024) 026 [arXiv:2310.04405] [INSPIRE].

[85] R. Aoude, K. Haddad, C. Heissenberg and A. Helset, *Leading-order gravitational radiation to all spin orders*, *Phys. Rev. D* **109** (2024) 036007 [arXiv:2310.05832] [INSPIRE].

JHEP11(2024)109

[86] P.S. Howe, S. Penati, M. Pernici and P.K. Townsend, *Wave Equations for Arbitrary Spin From Quantization of the Extended Supersymmetric Spinning Particle*, *Phys. Lett. B* **215** (1988) 555 [INSPIRE].

[87] F. Bastianelli, P. Benincasa and S. Giombi, *Worldline approach to vector and antisymmetric tensor fields*, *JHEP* **04** (2005) 010 [hep-th/0503155] [INSPIRE].

[88] F. Bastianelli, P. Benincasa and S. Giombi, *Worldline approach to vector and antisymmetric tensor fields. II*, *JHEP* **10** (2005) 114 [hep-th/0510010] [INSPIRE].

[89] S. Abreu et al., *Caravel: a C++ framework for the computation of multi-loop amplitudes with numerical unitarity*, *Comput. Phys. Commun.* **267** (2021) 108069 [arXiv:2009.11957] [INSPIRE].

[90] F.A. Berends and W.T. Giele, *Recursive Calculations for Processes with n Gluons*, *Nucl. Phys. B* **306** (1988) 759 [INSPIRE].

[91] D. Brizuela, J.M. Martin-Garcia and G.A. Mena Marugan, *xPert: computer algebra for metric perturbation theory*, *Gen. Rel. Grav.* **41** (2009) 2415 [arXiv:0807.0824] [INSPIRE].

[92] T. Nutma, *xTras: a field-theory inspired xAct package for mathematica*, *Comput. Phys. Commun.* **185** (2014) 1719 [arXiv:1308.3493] [INSPIRE].

[93] G. Ossola, C.G. Papadopoulos and R. Pittau, *Reducing full one-loop amplitudes to scalar integrals at the integrand level*, *Nucl. Phys. B* **763** (2007) 147 [hep-ph/0609007] [INSPIRE].

[94] R.K. Ellis, W.T. Giele and Z. Kunszt, *A Numerical Unitarity Formalism for Evaluating One-Loop Amplitudes*, *JHEP* **03** (2008) 003 [arXiv:0708.2398] [INSPIRE].

[95] C.F. Berger et al., *An Automated Implementation of On-Shell Methods for One-Loop Amplitudes*, *Phys. Rev. D* **78** (2008) 036003 [arXiv:0803.4180] [INSPIRE].

[96] W.T. Giele, Z. Kunszt and K. Melnikov, *Full one-loop amplitudes from tree amplitudes*, *JHEP* **04** (2008) 049 [arXiv:0801.2237] [INSPIRE].

[97] R.K. Ellis, W.T. Giele, Z. Kunszt and K. Melnikov, *Masses, fermions and generalized D-dimensional unitarity*, *Nucl. Phys. B* **822** (2009) 270 [arXiv:0806.3467] [INSPIRE].

[98] H. Ita, *Two-loop Integrand Decomposition into Master Integrals and Surface Terms*, *Phys. Rev. D* **94** (2016) 116015 [arXiv:1510.05626] [INSPIRE].

[99] S. Abreu et al., *Two-Loop Four-Gluon Amplitudes from Numerical Unitarity*, *Phys. Rev. Lett.* **119** (2017) 142001 [arXiv:1703.05273] [INSPIRE].

[100] S. Abreu et al., *Planar Two-Loop Five-Gluon Amplitudes from Numerical Unitarity*, *Phys. Rev. D* **97** (2018) 116014 [arXiv:1712.03946] [INSPIRE].

[101] T. Peraro, *Scattering amplitudes over finite fields and multivariate functional reconstruction*, *JHEP* **12** (2016) 030 [arXiv:1608.01902] [INSPIRE].

[102] A. von Manteuffel and R.M. Schabinger, *A novel approach to integration by parts reduction*, *Phys. Lett. B* **744** (2015) 101 [arXiv:1406.4513] [INSPIRE].

[103] S. Weinberg, *Infrared photons and gravitons*, *Phys. Rev.* **140** (1965) B516 [INSPIRE].

[104] P.V. Landshoff and J.C. Polkinghorne, *Iterations of regge cuts*, *Phys. Rev.* **181** (1969) 1989 [INSPIRE].

[105] J. Parra-Martinez, M.S. Ruf and M. Zeng, *Extremal black hole scattering at $\mathcal{O}(G^3)$: graviton dominance, eikonal exponentiation, and differential equations*, *JHEP* **11** (2020) 023 [arXiv:2005.04236] [INSPIRE].

JHEP11(2024)109

[106] A. Luna, I. Nicholson, D. O'Connell and C.D. White, *Inelastic Black Hole Scattering from Charged Scalar Amplitudes*, *JHEP* **03** (2018) 044 [arXiv:1711.03901] [INSPIRE].

[107] C. Cheung, I.Z. Rothstein and M.P. Solon, *From Scattering Amplitudes to Classical Potentials in the Post-Minkowskian Expansion*, *Phys. Rev. Lett.* **121** (2018) 251101 [arXiv:1808.02489] [INSPIRE].

[108] Z. Bern et al., *Black Hole Binary Dynamics from the Double Copy and Effective Theory*, *JHEP* **10** (2019) 206 [arXiv:1908.01493] [INSPIRE].

[109] C. Cheung, N. Shah and M.P. Solon, *Mining the Geodesic Equation for Scattering Data*, *Phys. Rev. D* **103** (2021) 024030 [arXiv:2010.08568] [INSPIRE].

[110] R.U. Sexl and H.K. Urbantke, *Relativity Groups, Particles. : Special Theory of Relativity as the Basis of Field and Elementary Particle Physics*, Springer, Wien (1976) [DOI:10.1007/978-3-7091-6234-7] [INSPIRE].

[111] D. Akpinar et al., *Spinning Black Hole Scattering at $\mathcal{O}(G^3S^2)$: Casimir Terms, Radial Action and Hidden Symmetry*, arXiv:2407.19005 [INSPIRE].

[112] J. Gluza, K. Kajda and D.A. Kosower, *Towards a Basis for Planar Two-Loop Integrals*, *Phys. Rev. D* **83** (2011) 045012 [arXiv:1009.0472] [INSPIRE].

[113] R.M. Schabinger, *A New Algorithm For The Generation Of Unitarity-Compatible Integration By Parts Relations*, *JHEP* **01** (2012) 077 [arXiv:1111.4220] [INSPIRE].

[114] K.J. Larsen and Y. Zhang, *Integration-by-parts reductions from unitarity cuts and algebraic geometry*, *Phys. Rev. D* **93** (2016) 041701 [arXiv:1511.01071] [INSPIRE].

[115] S. Abreu et al., *Two-Loop Four-Graviton Scattering Amplitudes*, *Phys. Rev. Lett.* **124** (2020) 211601 [arXiv:2002.12374] [INSPIRE].

[116] M. Abramowitz and I.A. Stegun, *Handbook of mathematical functions: with formulas, graphs, and mathematical tables*, vol. 55, Courier Corporation (1964).

[117] M. Beneke and V.A. Smirnov, *Asymptotic expansion of Feynman integrals near threshold*, *Nucl. Phys. B* **522** (1998) 321 [hep-ph/9711391] [INSPIRE].

[118] V.A. Smirnov and E.R. Rakhmetov, *The strategy of regions for asymptotic expansion of two loop vertex Feynman diagrams*, *Theor. Math. Phys.* **120** (1999) 870 [hep-ph/9812529] [INSPIRE].

[119] R.N. Lee, *Presenting LiteRed: a tool for the Loop InTEgrals REDuction*, arXiv:1212.2685 [INSPIRE].

[120] R.N. Lee, *LiteRed 1.4: a powerful tool for reduction of multiloop integrals*, *J. Phys. Conf. Ser.* **523** (2014) 012059 [arXiv:1310.1145] [INSPIRE].

[121] S. Abreu et al., *Analytic Form of Planar Two-Loop Five-Gluon Scattering Amplitudes in QCD*, *Phys. Rev. Lett.* **122** (2019) 082002 [arXiv:1812.04586] [INSPIRE].

[122] G.U. Jakobsen, *Gravitational Scattering of Compact Bodies from Worldline Quantum Field Theory*, Ph.D. thesis, Humboldt University, Berlin, Germany (2023) [arXiv:2308.04388] [INSPIRE].

[123] I.I. Shapiro, *Fourth Test of General Relativity*, *Phys. Rev. Lett.* **13** (1964) 789 [INSPIRE].

[124] S. Abreu, R. Britto, C. Duhr and E. Gardi, *Diagrammatic Hopf algebra of cut Feynman integrals: the one-loop case*, *JHEP* **12** (2017) 090 [arXiv:1704.07931] [INSPIRE].

JHEP11(2024)109

[125] J. Vines, J. Steinhoff and A. Buonanno, *Spinning-black-hole scattering and the test-black-hole limit at second post-Minkowskian order*, *Phys. Rev. D* **99** (2019) 064054 [arXiv:1812.00956] [INSPIRE].

[126] T. Damour, *Classical and quantum scattering in post-Minkowskian gravity*, *Phys. Rev. D* **102** (2020) 024060 [arXiv:1912.02139] [INSPIRE].

[127] S. Abreu et al., *Analytic Form of the Planar Two-Loop Five-Parton Scattering Amplitudes in QCD*, *JHEP* **05** (2019) 084 [arXiv:1904.00945] [INSPIRE].

[128] M. Heller and A. von Manteuffel, *MultivariateApart: generalized partial fractions*, *Comput. Phys. Commun.* **271** (2022) 108174 [arXiv:2101.08283] [INSPIRE].

[129] X. Liu and Y.-Q. Ma, *AMFlow: a mathematica package for Feynman integrals computation via auxiliary mass flow*, *Comput. Phys. Commun.* **283** (2023) 108565 [arXiv:2201.11669] [INSPIRE].

[130] S. Borowka et al., *pySecDec: a toolbox for the numerical evaluation of multi-scale integrals*, *Comput. Phys. Commun.* **222** (2018) 313 [arXiv:1703.09692] [INSPIRE].

[131] F. Teng and R. Roiban, private correspondence, (Dec. 2023).

[132] A. Brandhuber, G.R. Brown, G. Chen, S. De Angelis, J. Gowdy and G. Travaglini, private correspondence (Dec. 2023).

[133] A. Georgoudis, C. Heissenberg and I. Vazquez-Holm, *Addendum to: inelastic exponentiation and classical gravitational scattering at one loop*, *JHEP* **02** (2024) 161 [arXiv:2312.14710] [INSPIRE].

[134] G.U. Jakobsen, G. Mogull, J. Plefka and B. Sauer, *All things retarded: radiation-reaction in worldline quantum field theory*, *JHEP* **10** (2022) 128 [arXiv:2207.00569] [INSPIRE].

[135] X. Liu, Y.-Q. Ma and C.-Y. Wang, *A Systematic and Efficient Method to Compute Multi-loop Master Integrals*, *Phys. Lett. B* **779** (2018) 353 [arXiv:1711.09572] [INSPIRE].

[136] X. Liu and Y.-Q. Ma, *Multiloop corrections for collider processes using auxiliary mass flow*, *Phys. Rev. D* **105** (2022) L051503 [arXiv:2107.01864] [INSPIRE].

[137] Z.-F. Liu and Y.-Q. Ma, *Automatic computation of Feynman integrals containing linear propagators via auxiliary mass flow*, *Phys. Rev. D* **105** (2022) 074003 [arXiv:2201.11636] [INSPIRE].

[138] C. Duhr and F. Dulat, *PolyLogTools — polylogs for the masses*, *JHEP* **08** (2019) 135 [arXiv:1904.07279] [INSPIRE].

JHEP11(2024)109